THE IIOAB JOURNAL

VOLUME 11 : NO 3 : JULY 2020 : ISSN 0976-3104

Institute of Integrative Omics and Applied Biotechnology Journal

Dear Esteemed Readers, Authors, and Colleagues,

I hope this letter finds you in good health and high spirits. It is my distinct pleasure to address you as the Editor-in-Chief of Integrative Omics and Applied Biotechnology (IIOAB) Journal, a multidisciplinary scientific journal that has always placed a profound emphasis on nurturing the involvement of young scientists and championing the significance of an interdisciplinary approach.

At Integrative Omics and Applied Biotechnology (IIOAB) Journal, we firmly believe in the transformative power of science and innovation, and we recognize that it is the vigor and enthusiasm of young minds that often drive the most groundbreaking discoveries. We actively encourage students, early-career researchers, and scientists to submit their work and engage in meaningful discourse within the pages of our journal. We take pride in providing a platform for these emerging researchers to share their novel ideas and findings with the broader scientific community.

In today's rapidly evolving scientific landscape, it is increasingly evident that the challenges we face require a collaborative and interdisciplinary approach. The most complex problems demand a diverse set of perspectives and expertise. Integrative Omics and Applied Biotechnology (IIOAB) Journal has consistently promoted and celebrated this multidisciplinary ethos. We believe that by crossing traditional disciplinary boundaries, we can unlock new avenues for discovery, innovation, and progress. This philosophy has been at the heart of our journal's mission, and we remain dedicated to publishing research that exemplifies the power of interdisciplinary collaboration.

Our journal continues to serve as a hub for knowledge exchange, providing a platform for researchers from various fields to come together and share their insights, experiences, and research outcomes. The collaborative spirit within our community is truly inspiring, and I am immensely proud of the role that IIOAB journal plays in fostering such partnerships.

As we move forward, I encourage each and every one of you to continue supporting our mission. Whether you are a seasoned researcher, a young scientist embarking on your career, or a reader with a thirst for knowledge, your involvement in our journal is invaluable. By working together and embracing interdisciplinary perspectives, we can address the most pressing challenges facing humanity, from climate change and public health to technological advancements and social issues.

I would like to extend my gratitude to our authors, reviewers, editorial board members, and readers for their unwavering support. Your dedication is what makes IIOAB Journal the thriving scientific community it is today. Together, we will continue to explore the frontiers of knowledge and pioneer new approaches to solving the world's most complex problems.

Thank you for being a part of our journey, and for your commitment to advancing science through the pages of IIOAB Journal.

Yours sincerely,

Vasco Azevedo

Vasco Azevedo, Editor-in-Chief
Integrative Omics and Applied Biotechnology
(IIOAB) Journal

IIOAB JOURNAL

ARTICLE

METHODS OF LEFT-SIDED DISPLACEMENT TREATMENT OF THE ABOMASUM IN COWS AND FIRST HEIFERS IN TYUMEN REGION

Otto K. Sintiurev*, Larisa A. Glazunova, Andrei V. Plakhotnik, Iurii V. Glazunov, Olga A. Dragich, Klavdiia A. Sidorova

Department of Anatomy and Physiology FSBEI HE Northern Trans-Ural SAU, RUSSIA

ISSN 0976-3104

ABSTRACT

Read displacement is an acutely progressing disease, which is characterized by a change in the anatomical position of the abomasum, filled with gases, liquid their combination, right or left. The aim of the research is to compare the effectiveness of various methods of surgical treatment of left-sided abomasum displacement in cows. Surgical treatment of left-sided displacement of the abomasum by "puncture", "suturing through the paralumbal fossa", and "abdominal midline operation" were used. It was established that abomasum displacement is recorded in 4.39% of cows and first heifers of the surveyed farm. In total, 75 first heifers and 31 cows were operated. It was found that each of the methods had both advantages and disadvantages. Given the advantages and disadvantages of each of the compared methods of treatment, as well as a high incidence of left-sided displacement of the abomasum among the first heifers, it is most advisable to use a puncture method that is simple to perform, quick to implement, low invasive, ensures low recurrence rate and high efficiency. In case of sufficient experience of the doctor and the capabilities of the farm facilities for the surgical treatment of cows and first heifers, treatment by suturing through the paralumbal fossa can be recommended.

KEY WORDS
cows, first heifers, abomasum displacement, ultrasound arouse, puncture method, paralumbal fossa

INTRODUCTION

Read displacement is an acutely progressing disease, which is characterized by a change in the anatomical position of the abomasum, filled with gases, liquid their combination, right or left [1, 2]. At left-sided displacement, the abomasum is located caudodorsally between the scar and the left abdominal wall, and at right-sided - between the right abdominal wall and the intestine [3]. Left-sided displacement of the abomasum is characteristic of Holstein-Friesian cows and is recorded in 3-8% of the stock [4,5,6]. Right-sided displacement of the abomasum occurs much less frequently and is much easier to diagnose by rectal examinations [7]. A heavily enlarged abomasum is located between the abdominal wall and the intestinal loops, reaching the right paralumbal fossa [3]. Since conservative treatment ensures practically no results, and valuable animals drop out of the herd, the damage from the disease is enormous and consists of loss of milk production, which reaches 30%, as well as premature disposal of sick animals or their death [6, 8-10].

Since 2005, Holstein-Frisian cattle have been imported to Tyumen region, which today forms the basis of the entire dairy herd of the region. In this regard, the problem of the abomasum displacement is relevant and needs to be addressed. Since conservative treatment has low efficacy and does not provide for the complete recovery of the animal, we set a goal to compare the effectiveness of various methods of surgical treatment of left-sided abomasum displacement in cows.

Received: 22 Jan 2020
Accepted: 19 Mar 2020
Published: 2 Apr 2020

MATERIALS AND METHODS

The study was conducted from February 2015 to March 2017 in the breeding plant ZapSibKhleb-Iset LLC of Isetsky district of Tyumen region. During the observation period, 2,460 cows with a productivity of 8,000 kg per year per 1 fodder cow were examined. The farm uses a stable-outdoor housing and a loose housing of animals.

To diagnose displacement, the data of anamnesis and the main symptoms were considered and other diseases of the internal organs with characteristic clinical manifestations were excluded. To diagnose the left-sided displacement of the abomasum, a method of visual assessment of the animal was used, since cows with this pathology strongly lose their weight. With the help of percussion, a basket-ball-bouncing sound was detected, the tone of this sound may vary depending on the course of the disease. During auscultation of the abomasum displacement areas were determined by sounds of fluid overflow; sometimes the sound of a falling drop was recorded. Rectal examination allowed finding location of the abomasum. Thus, a greatly enlarged abomasum could be located between the abdominal wall and intestinal loops, near the right or left paralumbal fossa [3, 11].

Despite the use of standard research methods, 15% of cases of left-side displacement of the abomasum cannot be or rarely determined by auscultation. Auscultation with the help of a stethoscope is often complicated by industrial noise, which can prevent to find the best sound point and affect the outcome of the operation. Rectal examination also can be uncertain due to the different habit of animals. Thus, it is quite difficult to determine the correct abomasum topography with rectal examination in large animals. In this regard, for a more accurate diagnosis of abomasum displacement, a need for ultrasound arouse. For

***Corresponding Author**
Email:
otto.sintyurev@yandex.ru

IIOAB JOURNAL
ISSN: 0976-3104

this purpose, DRAMINSKI ultrasonic scanner with a convex sensor, scanning depth 15 cm and frequency 7.5 MHz was used;

The study used Mediagel highly-viscous ultrasound gel, which provided the optimal viscosity for the best visualization of the test organ. Ultrasound examination was performed in various positions of the animal: in the standing position, fixed in the machine, and fixed in the dorsal position.

During the operation by the puncture method, the animal was fixed in the dorsal position; the best points of hearing the abomasum and for puncture were determined by percussion, auscultation or ultrasound examination revealed. The surgical field was prepared and, in the area of the best sound localization, the abdominal wall and the abomasum were punctured using the trocar cannula, while trying to avoid disrupting the integrity of the intra-abdominal and hypodermic veins and blood vessels. After the puncture, the trocar was removed, leaving a cannula in a perforated abomasum. An indicator of perforation was the characteristic odor of abomasum gas. The suture fixator was inserted through the cannula into the abomasum using a trocar, then the cannula was removed, leaving the suture. Exactly the same principle was used to make a puncture at a distance of 7 cm. The seams were tied 5 cm from the skin surface. An antiseptic wound treatment was performed and the animal was turned on its left side and forced to stand. After the operation, 40 liters of warm water with energy drink was fed to the animal with the help of a drencher. After surgery, a diet was prescribed [12-20].

During surgical treatment by suturing through the paralumbal fossa, the animal was fixed in a standing position, in a cage or machine, with the head securely fixed and the pelvic limbs tied together. The surgical field was prepared. Anesthesia was provided with a conductive paralumbal blockade with 100 ml of a 0.5% novocaine solution, and infiltration anesthesia was performed with a 2% novocaine solution in the area for the incision. Laparotomy was performed in the left paralumbal fossa, bleeding was stopped as the layers of the abdominal wall were dissected. After opening, the arm entered the abdominal cavity and the palm went along the abdominal wall behind the last rib 20 cm below the lumbar transverse vertebrae or along the scar, in most cases the abomasum was visible in the wound. For better convenience, the abomasum was pulled closer to the surgical wound, a needle with a rubber tube was inserted into it in order to reduce the volume of gases and the abomasum size. Then the displaced abomasum was captured by hand and carefully tightened to the edge of the wound, and then stitched with ta wo-story suture. At the same time, the suture in the region of large curvature was applied 5-7 cm long, not touching the mucous membrane of the stomach, at the ends of the suture, threads were sutured 1.5-2 m long. Then the abdominal wall was pierced from the inside along the midline of 25 cm from the cartilage, and the abomasum was placed in the abdominal cavity. To do this, an assistant was involved, who gradually tightened the thread to fix the stomach. During physiological positioning of the abomasum the topography of other organs was monitored. After placing the organ in a correct position, the assistant fixed both ends of the thread at a distance of 8-10 cm from the skin surface. In order to avoid injury to the skin, under the fixing thread a bandage was tied between the skin and the thread. At the end of the operation, an antibiotic was administered and the wounds were sutured. After the operation, the animal was isolated and received 40 liters of water with propylene glycol and Lacto-rumen, was prescribed a diet, a course of antibiotics and symptomatic therapy. Sutures were removed after 7-10 days [10, 21-26].

During the abdominal medial surgery on the abomasum, the animal was fixed in the dorsal position, like for the puncture method. The operating field was prepared and the access point was anesthetized using an infiltration anesthesia with a 0.5% novocaine solution. A section located 20 cm from the cartilage was cut along the white line. After the laparotomy, the operating physician inserted his hand into the abdomen with a tubed needle used to reduce the pressure and size of the abomasum through the removal of gases from it. After this, the wall of the abomasum was sutured with a two-story suture to provide a reliable fixation of the stomach; suturing was performed to the caudal edge of the surgical wound. Amoxylong antibiotic was injected into the abdominal cavity and surgical wound was sutured with the subsequent treatment of the suture. After the operation, measures were taken as in the method of suturing through the paralumbal fossa [10, 21-26].

RESULTS

During the observation period at the farm, 108 cases of left-sided displacement of the abomasum were recorded, which was 4.39%. To confirm the diagnosis, an ultrasound examination was conducted. For this, the cow in a standing position was shaved its fur in the region of the left hypochondria, namely in the region of the two last ribs, after which the gel was applied and the abdominal cavity was scanned, in particular, the abomasum [Fig. 1].

As [Fig. 1] shows, the ultrasound examination sowed a hyperechoic zone, which is characteristic of this pathology. Hyperechoicity is explained by the presence of gas formed in the abomasum and the very high pressure caused by it, which makes the ultrasound glow.

Fig. 1: The boundary line between the abomasum and abdominal cavity.

Ultrasound examination in supine position was performed in the upper abdomen, as well as during auscultation.

In the course of the study, an image was obtained showing the hyperechoic glowing emitted by the contents of the abomasum [Fig. 2]. During the operation by puncture method, invasive intervention (puncture) was performed in places where the glow of gases was the most intense.

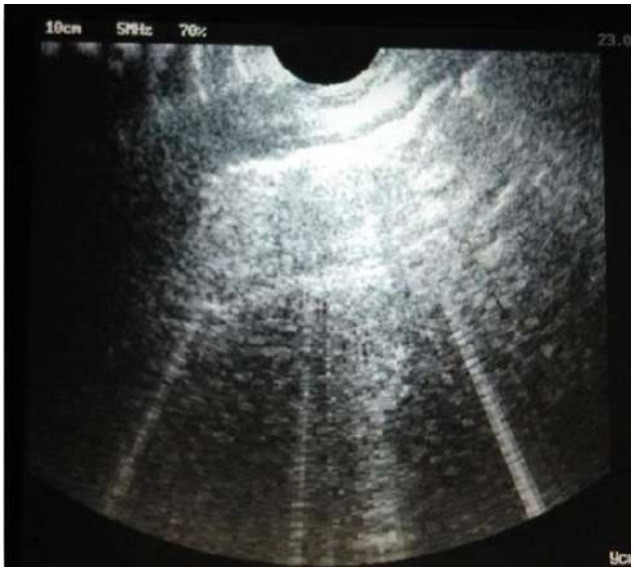

Fig. 2: The boundary line between the abomasum and abdominal cavity immediately before the surgical intervention.

It has been established that the use of ultrasound examination in the case of displacement of the abomasum in cows as well as traditional methods does not ensure 100% effectiveness. Nevertheless, ultrasound allows accurately determining the intensity of the pathological process, with minimal impact of external factors affecting the quality of this diagnosis and the establishment of localization of surgical intervention.

In case of surgical treatment of the abomasum displacement in our work, we stopped at the three main surgical methods, namely the method of "puncture", the method of “suturing through the paralumbal fossa", and the method of "abdominal medial surgery".

The main tasks of each method is to return the abomasum to its physiologically correct position, and to ensure its reliable attachment. For an objective assessment of the efficacy of surgical treatment, we divided the ill animals into two groups: first heifers and cows.

The results of the treatment of the abomasum displacement are presented in [Table 1 and Table 2].

IIOAB JOURNAL
ISSN: 0976-3104

It was established that the greatest degree of pathology is recorded in the first heifers. Thus, the occurrence of the left-sided displacement of the abomasum during the study period was observed in 75 first heifers and 31 cows.

During the study of the effectiveness of various methods of surgical treatment of the abomasum displacement, we noted both the advantages and disadvantages of each of the methods used.

Table 1: Effectiveness of various methods of surgical treatment of left-sided displacement of the abomasum in first heifers

Indicator	Method of treatment		
	Puncture method	Suturing through the paralumbal fossa	Abdominal medial surgery
Number of experimental animals, total	68	4	3
Animal healed, un.	57	3	2
Efficacy of treatment, %	83.82	75.00	66.67
Recurrent displacement, un.	11	0	0
Disposed as a result of complications, un.	4	1	1
%	5.88	25.00	33.33

Table 2: Effectiveness of various methods of surgical treatment of left-sided displacement of the abomasum in cows

Indicator	Method of treatment		
	Puncture method	Suturing through the paralumbal fossa	Abdominal medial surgery
Number of experimental animals, total	27	3	1
Animal healed, un.	22	3	0
Efficacy of treatment, %	81.48	100.00	0
Recurrent displacement, un.	5	0	0
Disposed as a result of complications, un.	4	0	1
%	14.82	0	100.00

Thus, the advantages of the puncture method are simplicity, due to the minimum access, quickness of the manipulations and minimum costs of treatment, while the success of the operation was 81.32% and 81.48% in the treatment of first heifers and cows, respectively. The disadvantages of this method include poor guidance during the operation (the abomasum is not visible), as well as inconvenient fixation of the animal (in the supine position).

Surgical treatment with suturing through the paralumbal fossa was characterized by a high success rate among experienced surgeons, a comfortable position of the animal during the operation (in a standing position), no relapses, visual access to the operated organ and direct suturing of the abomasum, and control of fixation. The disadvantages of this method include a large surgical wound and the associated long-term postoperative recovery. It should be noted that the surgeon operating the animal must have certain physical characteristics subject to the long duration of the operation and need for physical strength and endurance, as well as long arms to grip the abomasum through the entire abdominal cavity.

The midline abdominal surgery is similar to puncture method and has a number of advantages, such as visualization of the abomasum, which allows it to be securely fixed, and fixing the animal in the dorsal position contributes to displacement of the abomasum to its anatomical position. Among the drawbacks are uncomfortable for the animal fixation in the dorsal position, and stress which can provoke an emetic reflex during operation. The use of abdominal surgery requires a long postoperative recovery, as well as an extensive surgical wound to access and, despite this, the impossibility of examining part of the abdominal cavity in this position.

CONCLUSION

Given the advantages and disadvantages of each of the compared methods of treatment, as well as a high incidence of left-sided displacement of the abomasum among the first heifers, it is most advisable to use a puncture method that is simple to perform, quick to implement, low invasive, ensures low recurrence rate and high efficiency (81.32% in first heifers and 81.48% in cows). In case of sufficient experience of the doctor and the capabilities of the farm facilities for the surgical treatment of cows and first heifers, treatment by suturing through the paralumbal fossa can be recommended.

CONFLICT OF INTEREST
There is no conflict of interest.

ACKNOWLEDGEMENTS
None.

FINANCIAL DISCLOSURE
None.

REFERENCES

[1] Niehaus AJ. [2008] Surgery of the Abomasum. Vet Clin North Am Food Anim Pr, 24:349-358.
[2] [2004] Trent A.: Surgery of the abomasum. Farm animal surgery. WB Saunders Co, 196-239.
[3] Anderson D, Gaughan E. [1993] Normal laparoscopic anatomy of the bovine abdomen. Am J Vet Res, 54:1170-1176.
[4] Jorritsma R, Westerlaan B, Bierma MPR, Frankena K. [2008] Milk yield and survival of Holstein-Friesian dairy cattle after laparoscopic correction of left-displaced abomasum. Vet Rec, 162:743-746.
[5] Newman KD, Anderson DE, Silveira F. [2005] One-step laparoscopic abomasopexy for correction of left-sided displacement of the abomasum in dairy cows. J Am Vet Med Assoc, 227:1142-1147.
[6] Raizman EA, Santos JEP. [2002] The effect of left displacement of abomasum corrected by toggle-pin suture on lactation, reproduction, and health of Holstein dairy cows. Journal of dairy Science, 5:1157-1164.
[7] Mordak R, Nicpoń J. [2015] Metabolic conditions of displacement of abomasum in cows. Med Weter, 71:142-145.
[8] Chasovshchikova MA, Sheveleva OM, Svjazhenina MA, Tatarkina NI, et al. [2017] Relationship between the genetic variants of kappa-casein and prolactin and the productive-biological characteristics of cows of the black-motley breed. Journal of Pharmaceutical Sciences and Research, 9(7):1038-1044.
[9] Glazunova LA, Glazunov YuV, Ergashev AA. [2018] Ecological-epizootical situation on telasiosis among large cattle in Northern Ural region. Research Journal of Pharmaceutical, Biological and Chemical Sciences, 9(4):1687-1693.
[10] Van W, SCL, Kuiper R. Left displacement of the abomasum in dairy cattle: recent developments in epidemiological and etiological aspects. Veterinary Research, 34(1):47-56.
[11] Barisani C. [2004] Evolution of Janowitz technique for abomasal dislocation therapy according to Barisani [dairy cows]. Summa, 5:35-39.
[12] Babkine M, Desrochers A, Bouré L, Hélie P. [2006] Ventral laparoscopic abomasopexy on adult cows. Can Vet J, 47:343-348.
[13] Connell J. [1976] Four Methods of Surgical Correction of Abomasal Displacement in the Cow. Iowa State Vet, 38:21-24.
[14] Freick M. [2013] Laparoscopic reposition of the displaced abomasum in a dairy herd in Saxony – a case series. Tierarztl Umsch, 8:311-321.
[15] Gnemmi G, Maraboli C. [2006] Bovine endoscopy: left abomasal dislocation: one step endoscopic approach with animal in quadrupedal station: retrospective evaluation Summa, 1:11-21.
[16] Gnus M, Ratajczak K, Antosik P. [2018] Application of a laparoscopic spieker of own design in reposition and fixation of the left displacement of the abomasum (LDA) in cattle. Medycyna weterynaryjna, 74(1):6059-2018.
[17] Janowitz H. [1998] Laparoscopic reposition and fixation of the left displaced abomasum in cattle. Tierarztl Prax Ausg G Grosstiere Nutztiere, 26:308-313.
[18] Mulon PY, Babkine M, Desrochers A. [2006] Ventral Laparoscopic Abomasopexy in 18 Cattle with Displaced Abomasum. Vet Surg. 35:347-355.
[19] Roy JP, Harvey D, Bélanger AM, Buczinski S. [2008] Comparison of 2-step laparoscopy-guided abomasopexy versus omentopexy via right flank laparotomy for the treatment of dairy cows with left displacement of the abomasum in on-farm settings. J Am Vet Med Assoc,232:1700-1706.
[20] Sickinger M. [2014] Clinic`c decade of LDA endoscoppic repositioning techniques in cows. Vet Times, 22:18-20.
[21] Baird AN, Harrison S. [2001] Surgical Treatment of Left Displaced Abomasum. Compend Contin Educ Pr Vet, 23:102-109.
[22] Kelton DF, Garcia J, Guard CL. [1988] Bar suture (toggle pin) vs open surgical abomasopexy for treatment of left displaced abomasum in dairy cattle. J Am Vet Med Assoc, 193:557-559.
[23] Newman KD, Harvey D, Roy JP. [2008] Minimally invasive field abomasopexy techniques for correction and fixation of left displacement of the abomasum in dairy cows. Vet Clin North Am Food, 24:359-382.
[24] Staric J, Biricik HS, Aksoy G, Zadnik T. [2010] Surgical Treatment of Displaced Abomasum in Cattle Using Ljubljana Method. Acta Vet Brno, 79:469-473.
[25] Steiner A. [2006] Surgical treatment of the left displacement of the abomasum an update. XXIV World Buiatrics Congress, Nice, France.
[26] Trent A. [1990] Surgery of the bovine abomasum. Vet Clin North Am Food Anim Pract, 6:348-399.

ARTICLE

IMMUNE AND METABOLIC PARAMETERS OF BLOOD PLASMA AND ERYTHROCYTES AS QUALITY FACTORS OF ANTIBACTERIAL THERAPY IN PATIENTS WITH COMMUNITY-ACQUIRED PNEUMONIA

Polyakov D. V.*, Konoplya E. N., Mansimova O. V., Prokofeva Yu. V., Serikova L. N.

Department of Propaedeutics of Internal Diseases, Kursk State Medical University, Kursk, RUSSIA

ISSN 0976-3104

ABSTRACT

Community-acquired pneumonia (CAP) holds a dominate position in the structure of infections mortality factors in the world. Immune and metabolic disorders were studied before and after standard medical therapy in patients with community-acquired pneumonia. Laboratory criteria indicating immune inflammation, oxidative stress, endothelial dysfunction, and activation of lipid peroxidation were detected in the patients included in the study. Standard treatment does not normalize most of the altered parameters of the immune and metabolic status, which stipulates the necessity to search for the methods to correct the disorders by administering various combinations of preparations with immunomodulatory and antioxidant action in complex pharmacotherapy.

KEY WORDS
community-acquired pneumonia, immune inflammation, oxidative stress, endothelial dysfunction, lipid peroxidation

INTRODUCTION

Diseases of the respiratory system (DRS) consistently occupy a leading position in the structure of the overall morbidity among the population of the Russian Federation, accounting in 2014 29 455 225 cases (54.2% of all diseases) in children, 3 403 (33.2%) in adolescents, 23 394 842 (13.6%) - in adults [1- 3]. According to the World Health Organization report, in 2012 due to the development of lower respiratory tract infection (LRTI) 3.1 million people died [4]. Severe LRTIs rank third among the leading causes of death, conceding only to coronary heart disease, stroke, and other cerebrovascular diseases. Besides, the findings of the research show a change in the nature of the course, frequent development of complications and an increase in mortality in CAP [5].

Community-acquired pneumonias (CAPs) are one of the most common infectious diseases in the world and the Russian Federation [2]. M. Rosenbaum et al. provide data on the epidemiology of pneumonia in Europe and North America. Among adults, pneumonia occurs in 5-10 people per 1,000 population [3]. CAP morbidity in the developed countries varies from 1 to 11.6‰ among young and middle age and from 25 to 44‰ in people aged 65 and older [2]. According to Federal Oversight Service for Consumers' Right and Human Welfare, the incidence of CAP in Russia in 2014 accounted 337,77 cases per 100 thousand adult population [4]. About 400 thousand people are administered to hospitals of the country; in 2014 a little more than 40 thousand people died from pneumonia [3].

Received: 26 Jan 2020
Accepted: 21 Mar 2020
Published: 8 Apr 2020

Medical statistics data over the country lay emphasis on the immediacy of the problem in Russian healthcare system. If we summarize and compare them with international epidemiological studies, we can state the following: approximately 1 million people are not timely diagnosed with pneumonia, and mortality from severe forms of pneumonia has reached 10% [3].

Immune mechanisms are known to have an important role in the development and resolution of almost all pathological conditions, especially those with an infectious etiology, upon that the relationship between metabolic and immunological changes is well described. A mass and virulent infection, a decrease in nonspecific resistance of the organism, an imbalance of local and systemic immunity, a disturbance of free-radical oxidation processes play a leading role in CAP pathogenesis [5]. It is obvious that the timely and adequate administration of antimicrobial drugs, as the indicators of medical care quality, is the fundamental factor in the management of CAP patients. The immune system dysfunctions are manifested by hypo- and/or hyperactive processes and are one of the causes of the disease development [6, 7]. In this case, hypoactivation is associated with either a quantitative and functional insufficiency of the immune system components, or with the absence of full activation to a specific pathogen. The development of hyperactive conditions is associated with an increase in the quantitative and functional characteristics of the immune system effector components and/or insufficiency of suppressor factors [8]. It is such dysfunctional features or their combinations that underlie the development of infectious diseases [9, 10]. In this regard, immunological assessment of standard antibiotic therapy effectiveness is a general indicator of the therapy. Nevertheless, there are very few comprehensive researches devoted to the study of the immune and metabolic status not only prior, but also after the standard treatment [11- 16].

The aim of the study is to detect immune and metabolic disorders before and after standard treatment in patients with community-acquired bacterial pneumonia.

***Corresponding Author**
Email:
dima-polaykov@mail.ru

IIOAB JOURNAL
ISSN: 0976-3104

MATERIALS AND METHODS

Based on the conducted screening, 46 patients with community-acquired bacterial pneumonia were enrolled in the examination in the pulmonary department of the non-governmental healthcare institution "Department Hospital at the station Kursk "Russian Railways". Clinical observations were of controlled prospective open randomized study in nature. The general characteristics of the patients examined and the representation of concomitant pathology are shown in [Table 1]. Written consent from the subjects was taken and the study was approved by the Kursk State Medical University ethical committee.

Inclusion criteria: the patients under 18 are not included, CAP diagnosis made on the basis of epidemiological, clinical-radiological and laboratory data typical for this disease [17-19]. CAP diagnosis was made according to Russian National Recommendations for CAP and the recommendations of American Thoracic Society/Infectious Diseases Society of America [20- 22].

Patients with aspiration pneumonia, atypical pneumonia, viral pneumonia, nosocomial pneumonia, pulmonary tuberculosis, primary or metastatic lung cancer, cystic fibrosis, hepatic and/or renal failure, with severe concomitant diseases, with acute respiratory disorders, and those taking immunomodulatory agents for the preceding year were excluded from the study.

The control group consisted of practically healthy individuals (n = 18), consistent with the patients by sex and age.

Table 1: General characteristic of the patients examined

Clinical-anatomical characteristics		Patients included in the study
Sex (number of patients / percent)	Males	21 / 45,7
	Females	25 / 54,3
Mean age (years)		47,03±3,2 (from 20 to 77)
Disease duration (days) at out-patient treatment stage		8,23±1,05
Antibacterial therapy used at out-patient treatment stage (number of patients / percent)		20 / 43,4
First hospital admission with CAP diagnosis (number of patients / percent)		46 / 100
Smoking (number of patients / percent)		18 / 39,1
Smoking index (for smoking patients)		15,7
Comorbid conditions (number of patients / percent)		34 / 73,9
Upper respiratory tract diseases (number of patients / percent)		11 / 23,9
Characteristic of egocentric and objective status on admission (number of patients / percent)	Chest pain	37 /80,4
	Cough	46 /100
	Dyspnea (scores)	3,47±0,47
	Body temperature	38±0,12
	Respiratory rate	21,97±0,92

Table 2: Characteristic of patients concerning CAP severity

Indicants	Patients included in the study
CRB-65 (scores)	0,53±0,13
SMRT-CO (scores)	0,53±0,12

According CAP severity was determined in accordance with clinical guidelines [23]. To collect clinical and laboratory data, we used specially designed case registration forms which included demographic data, diagnosis, medical history, physical findings, results of laboratory and instrumental research methods. Mortality prediction estimation was made by CRB-65 scale [24]. Identification of patients requiring intensive respiratory support and vasoconstrictors infusion was carried out by SMRT-CO scale [23]. To interpret these scales data, the assessment of the following parameters was involved: age, impairment of consciousness, respiratory rate, systolic and diastolic blood pressure, chest X-ray findings, heart rate. Prognosis and severity of the disease assessment was performed upon the patient's admission, on the 3rd, 7th day of ward treatment and at time of hospital discharge. Characteristics of the study group in relation to the underlying pathology severity are presented in [Table 2].

Assessment of clinical laboratory data in the main groups was carried out on the 1st and 10th day of therapy. Erythrocytes and plasma were obtained from 10 ml of heparinized blood, for this purpose plasma was separated after its centrifugation, and packed erythrocytes were twice precipitated in 20 ml of 10 mM Na-phosphate buffer (pH = 7.4) containing 0.9% sodium chloride and 3% dextran T-500 for 30 minutes at 37°C.

IIOAB JOURNAL
ISSN: 0976-3104

After centrifugation, the supernatant fluid was removed by aspiration, and the packed erythrocytes were subjected to additional purification by chromatographic column through HBS-cellulose.

The intensity of lipid peroxidation (LPO) processes was assessed by acyl hydroperoxides (AHP) and malondialdehyde (MDA) content in blood plasma and erythrocytes, which form a colored butanol-extractable iodine complex with thiobarbituric acid. To determine MDA and AHP, TBK-Agat kit (Agat-Med Russia), Apel-330 spectrophotometer (Japan) at the wavelength 535 nm and 570 nm were used. To assess the antioxidant system status, we used the method of direct/ competitive heterogeneous enzyme-linked immunosorbent assay (ELISA) with the detection of resultants in 405-630 wavelength range by ready-made commercial kits: superoxide dismutase (SOD) activity "Bender Medsystems" (Austria) and catalase activity "Cayman Chemical" (USA). Total antioxidant status (TAS) was determined by a method based on the inhibition degree of ascorbate- and ferro-induced tween-80 oxidation to MDA. The level of stable metabolites of nitric oxide (SMON) was detected by two analytical operations: measurement of endogenous nitrite and conversion of nitrate into nitrite using nitrite-reductase, followed by total nitrite measurement by absorption of azo dye in Griess reaction at the wavelength 540 nm using ELISA kit "R&D" (England). In addition, the levels of C-reactive protein (CRP) "Vector-Best" (Russia), neopterin "IBL" (Germany), erythropoetin "Biomerica" (USA) were determined in blood plasma. Ceruleoplasmin was determined by immune turbidimetry method using "Sentinel" kit (Spain).

The content of cytokines, complement components and their inhibitors was determined in the blood plasma. Interleukin 1β (IL-1β), interleukin 2 (IL-2), interleukin 4 (IL-4), interleukin 6 (IL-6), interleukin 8 (IL-8), interleukin 17 (IL-17), interleukin 18 (IL-18), gamma-interferon (IFNγ), interleukin 10 (IL-10), tumor necrosis factor (TNFα), interleukin-1 receptor antagonist (IL-1RA), granulocyte-macrophage colony-stimulating factor (G-CSF), complement components (C3, C3a, C4, C5, C5a) and immunoglobulins M, G, A (IgM, G, A) were detected by ELISA method using ZAO "Vector-Best" and OOO "Tsitokin" (Russia) sets. When determining inhibitors of the complement system, factor H concentration was established by OOO "Tsitokin" (Russia) diagnostic kit through two principles: hemolytic method for CS activation accounting and ELISA method to detect a terminal complex by specific antibodies, and C1-inhibitor activity (C1-inh.) was detected by the ability to inhibit C1-esterase. ELISA results registration was carried out by means of microplate photometer "Sunrise", Tecan (Austria).

Phagocytic activity of poly morphonucleocytes after their isolation from the blood on velocity sedimentation gradient ficoll-urografin (d = 1.077) was assessed determining the phagocytic index (PI), phagocytic number (FN) and phagocytosis activity index (PAI) [24]. The activity of oxygen-dependent neutrophil systems was assessed by PD 303 SApel (Japan) spectrophotometer through the reduction reaction of nitro-blue tetrazolium (NBT-test), spontaneous (NBT-sp.) and stimulated (NBT-st.), by zymosan, stimulation index (STI) and neutrophils functional reserve (NFR) [25].

In addition, immunological and metabolic parameters in plasma samples and peripheral blood erythrocytes of 18 healthy donors (38.2 ± 4.5 years old) that formed the control group were studied; the obtained results were taken for conditional norm.

Statistical processing of the research results was performed in accordance with generally accepted principles of statistical analysis. When comparing the quality parameters, we used the criterion $\chi 2$ (chi-square). To assess the polygenic character relationship to the type of distribution, we used Shapiro-Wilk statistics. To compare normally distributed values we used Student t-test. The estimation of statistical significance of differences for quantitative values with abnormal distribution was performed by means of Wilcoxon-Mann-Whitney test (when comparing dependent groups). Values of normally distributed quantitative parameters are presented by arithmetic mean (M) with mean deviation (m), and abnormally distributed – by median (Me) with interquartile interval (P25; P75). The relationships were established on the basis of factor analysis, cluster analysis and Spearman rank correlation. Statistically significant differences were considered at $p<0.05$.

RESULTS AND DISCUSSION

For correct interpretation of changes in egocentric and objective status of patients, prior to the analysis of immune and metabolic changes, indicators of routine prognostic scales were evaluated (Table 3). According to CRB-65 scale, a significant ($p <0.05$) reduction in the risk of adverse outcome occurs to the 7th day and the end of therapy. The results of SMRT-CO scale illustrate a significant reduction in the need for intensive respiratory support and vasoconstrictors infusion in order to maintain an adequate level of blood pressure to the 3d day of therapy ($p<0.05$) and an increase in positive changes to the 7th day ($p <0,01$) and the end of treatment ($p <0.001$).

In blood plasma of patients with CAP, prior to treatment, we established an increase in pro-inflammatory cytokines: TNFα, IL-1β, IL-6, IL-8, IL-17 and IL-18 by 4.8; 2.2; 2.9; 4.0; 1.5 and 2.3 times respectively, a decrease in anti-inflammatory cytokines: IL-4, IL-10 and IL-1RA by 1.8, 2.4 and 2.3 times respectively. The content of IFNγ, IL-2 and G-CSF growth factor turned out to be higher than those of healthy donors by 2.1; 25.7 and 7.0 times respectively. After conducted treatment, the concentrations of IL-4 and IL-10 returned to normal, the levels of IL-17 and IFNγ did not change, and the content of the other cytokines studied was corrected towards the values of healthy donors, but not to their values [Table 4].

Table 3: Shift table for CRB-65 and SMRT-CO scales in CAP patients

Indicants	Curation days				Statistical significance of differences
	I. 1st	II. 3d	III. 7th	IV. on hospital discharge	
CRB-65 (scores)	0,53±0,13	0,33±0,11	0,23±0,08	0,2±0,07	P I-II>0,05 P I-III<0,05 P I-IV<0,05 P II-III>0,05 P II-IV>0,05 P III-IV>0,05
SMRT-CO (scores)	0,53±0,12	0,27±0,09	0,13±0,06	0,03±0,03	P I-II<0,05 P I-III<0,01 P I-IV<0,001 P II-III>0,05 P II-IV<0,05 P III-IV>0,05

Table 4: Cytokine spectrum of blood plasma in patients with community-acquired pneumonia before and after standard treatment (M±m)

Indicants	Unit of measure	1 Healthy	2 Before therapy	3 Post-treatment period
TNFα	pkg/ml	3,81±0,92	18,23±1,08 *1	7,11±0,63 *1,2
IL-1β	pkg/ml	1,9±0,09	4,13±0,22 *1	3,6±0,08 *1,2
IL-6	pkg/ml	2,8±0,11	8,13±0,23 *1	6,43±0,32 *1,2
IL-8	pkg/ml	4,7±0,9	18,7±2,1 *1	10,3±1,41 *1,2
IL-17	pkg/ml	8,1±0,32	11,9±1,1 *1	10,02±1,02 *1
IL-18	pkg/ml	291,4±12,3	656,2±17,1 *1	585,5±14,7 *1,2
IL-4	pkg/ml	3,8±0,31	2,12±0,24 *1	4,3±0,23 *2
IL-10	pkg/ml	10,53±0,76	4,45±0,56 *1	11,3±0,55 *2
IL-1RA	pkg/ml	420,9±10,4	181,2±11,3 *1	220,3±9,72 *1,2
IFNγ	pkg/ml	4,65±0,41	9,87±2,13 *1	10,2±1,4 *1
IL-2	pkg/ml	0,21±0,01	5,4±0,32 *1	4,3±0,17 *1,2
G-CSF	pkg/ml	12,1±1,0	84,33±8,71 *1	65,3±4,4 *1,2

Note: here and in the tables below, an asterisk (*) indicates significant differences in arithmetic means (p <0.05); the figures next to the asterisk - in relation to which group indicators these differences are given

Table 5: Immune status parameters of blood in patients with community-acquired pneumonia before and after standard treatment (M±m)

Indicants	Unit of measure	1 Healthy	2 Before therapy	3 Post-treatment period
C_3	mg/dL	15,0±2,0	0,45±0,04 *1	0,42±0,02 *1
C_{3a}	ng/ml	50,1±4,3	21,52±0,71 *1	26,2±0,5 *1,2
C_4	mg/dL	12,1±2,7	0,27±0,01 *1	0,45±0,03 *1,2
C_5	mg/dL	8,3±0,9	0,69±0,04 *1	0,72±0,02 *1
C_{5a}	ng/ml	4,0±0,6	7,77±0,21 *1	5,83±0,55 *1,2
C_1-inh.	ng/ml	220,1±12,3	425,1±17,5 *1	245,0±20,2 *2
Factor H	ng/ml	78,3±10,4	80,5±12,31	69,67±13,7
IgM	mg/dL	26,04±3,92	29,94±3,95	19,8±3,84 *1,2
IgG	mg/dL	658,73±24,3	626,81±32,5	583,7±24,3 *1,2
IgA	mg/dL	177,68±38,16	332,29±26,99 *1	238,4±48,4 *1, 2
PI	%	74,3±2,3	66,8±1,93 *1	73,7±1,6 *2
PN	abs.	4,64±0,23	4,07±0,15 *1	4,88±0,2 *2
PAI	-	3,43±0,11	2,72±0,13 *1	3,6±0,2 *2
NBT-sp.	%	9,4±0,5	13,7±1,1 *1	11,4±0,72 *1,2
NBT-st.	%	22,3±2,04	27,8±2,0 *1	24,1±1,7
NFR	%	12,9±1,3	14,1±1,2	12,7±1,1
STI	-	2,37±0,12	2,03±0,1 *1	2,11±0,24

Upon hospital admission, among other paramours of immune status in CAP patients a decrease in the content of C3, C3a, C4, C5-complement components and C1-inhibitor by 33.3, 2.3, 44.8, 12.0 and 1.9 times respectively, an increase in C5a and IgA by 1.9 times were revealed, the level of factor H inhibitor remained within normal range. After the standard treatment, the C1-inhibitor concentrations returned to normal, C3a, C4, C5a and IgA levels were corrected in the direction of healthy donors, C3, C5-complement components and factor H level did not change, but the concentration of IgM and IgG decreased below the donor levels [Table 5].

When studying functional metabolic activity of peripheral blood neutrophils at the beginning of treatment, the following results were obtained: a decrease in indicators of phagocytosis activity and intensity (PI, PN and PAI) in comparison with healthy donors, an increase in activity parameters of polymorphonucleocytes oxygen-

IIOAB JOURNAL
ISSN: 0976-3104

dependent systems (NBT-sp., NBT-st.), in the absence of NFR changes and a decrease in STI. On treatment completion most of the studied parameters of neutrophils functional metabolic activity normalized, to the exclusion of corrected NBT-sp. test [Table 5].

In CAP patients, activation of peroxidation processes in blood plasma and erythrocytes was established prior to treatment (increased concentration of MDA by 5.5 and 10.4 times respectively and AHP by 7.7 and 10.5 times in blood plasma and erythrocytes), a decrease in antioxidant defense factors (TAS in plasma and erythrocytes by 1.2 times, ceruleoplasmin concentration in plasma by 1.3 times, SOD activity by 1.3 and 1.5 times, respectively, and catalase activity by 1.7 and 1.4 times) as well. In blood plasma and erythrocytes the level of SMON increased by 3.5 and 3.9 times, respectively. Besides, an increase in the concentration of erythropoietin by 2 times and inflammatory markers: neopterin by 1.5 times and CRP by 2.6 times was detected in blood plasma. After the treatment conducted, catalase activity in blood plasma and erythrocytes, ceruloplasmin level and SOD activity in the plasma normalized. Erythrocytes TAS remained unchanged, the other metabolic parameters studied shifted towards the level of healthy donors, without reaching their level [Tables 6, 7].

Thus, upon clinical admission of patients with CAP, 41 (91.1%) values were changed from the values of healthy donors out of 45 studied parameters of the immune and metabolic status. We can conclude that there are deep immune metabolic disorders that might be considered as immune inflammation, oxidative stress, endothelial dysfunction and activation of lipid peroxidation.

It is important to note that the course of conducted standard treatment, consisting of 10 days, did not normalize 70.7% of the studied laboratory immune metabolic parameters that had been changed before treatment and additionally reduced IgM and IgG content below the donors level in CAP patients cohort, which requires the administration of combined immunomodulatory and antioxidant therapy.

The presence of immune inflammation in the patients studied is confirmed by the increased level of TNFα, IL-1β, IFNγ, IL-17, activation marker of cellular immunity neopterin, and an increase in the level of C5a fragment-active chemotactic and vasodilator factor released by complement activation, that is anaphylactogenic in its activity.

Table 6: Metabolic parameters of blood plasma in patients with community-acquired pneumonia before and after standard treatment (M ± m)

Indicants	Unit of measure	1 Healthy	2 Before therapy	3 Post-treatment period
MDA	mcmol/l	0,92±0,03	5,1±0,28^{*1}	3,5±0,12^{*1,2}
AHP	c.u.	0,21±0,04	1,61±0,11^{*1}	0,71±0,05^{*1,2}
Catalase	mcat/l	21,7±0,27	12,86±0,48^{*1}	21,95±0,47^{*2}
SOD	c.u.	16,97±0,34	13,35±0,59^{*1}	20,37±0,67^{*1,2}
TAS	%	37,95±0,8	31,78±0,58^{*1}	39,19±0,45^{*2}
Ceruleoplasmin	g/l	0,32±0,04	0,24±0,03^{*1}	0,34±0,03^{*2}
Neopterin	pg/ml	6,02±0,15	4,06±0,11^{*1}	5,12±0,2^{*1,2}
CRP	mg/dL	3,7±0,27	9,54±0,69^{*1}	6,7±0,13^{*1,2}
SM_{NO}	mcmol/l	1,68±0,14	5,82±0,27^{*1}	3,93±0,1^{*1,2}
Erythropoetin	me/l	3,72±1,41	7,6±1,24^{*1}	2,6±0,29^{*1,2}

Table 7: Indicators of erythrocytes metabolism in patients with community-acquired pneumonia before and after standard treatment (M ± m)

Indicants	Unit of measure	1 Healthy	2 Before therapy	3 Post-treatment period
MDA	mcmol/l	0,32±0,03	3,34±0,1^{*1}	2,14±0,09^{*1,2}
AHP	c.u.	0,14±0,02	1,47±0,09^{*1}	0,87±0,06^{*1,2}
TAS	%	33,4±1,4	27,4±1,5^{*1}	28,5±1,32^{*1}
SOD	c.u.	19,23±1,62	12,41±1,02^{*1}	16,7±0,89^{*1,2}
Catalase	mcat/l	11,5±1,31	8,4±0,56^{*1}	10,3±1,2^{*2}
SM_{NO}	mcmol/l	1,12±0,04	4,34±0,12^{*1}	3,02±0,2^{*1,2}

and takes part in inflammation and hypersensitivity reactions with the absence of compensatory inhibitor increase (factor H) or even its decrease (C1-inh.) [13, 30, 31].

Oxidative stress development (imbalance between prooxidants and antioxidants, in which prooxidants predominate) is suggested in our studies by an increased concentration of LPO (MDA, AHP), SMON and CRP products (a marker of systemic inflammatory response) in plasma and erythrocytes, a significant decrease in antioxidant defense (TAS, SOD, catalase activity) [26, 27].

An increase in vasodilatory (ON) factor, an increased level of proinflammatory cytokines (TNFα, IL-1, IL-17), neopterin and CRP are indicative of endothelial dysfunction in patients with CAP [28- 30].

IIOAB JOURNAL
ISSN: 0976-3104

The obtained results show that laboratory immune metabolic disorders have been revealed in patients with CAP which is indicative of immune inflammation, oxidative stress, endothelial dysfunction, activation of lipid peroxidation. This establishes the necessity to intervene in the pathological process, to restore normal pulmonary tissue functioning and to reduce disabling effects. Conducted standard treatment does not normalize most of the altered parameters of the immune and metabolic status, which necessitates the search for agents able to correct the disorders by combined administration of various drugs with immunomodulatory and antioxidant effects in complex pharmacotherapy [3, 12].

CONFLICT OF INTEREST

There is no conflict of interest.

ACKNOWLEDGEMENTS

None.

FINANCIAL DISCLOSURE

None.

REFERENCES

[1] Bilichenko TN, Bystritskaна EV, Chuchalin AG, Belevskiy AS, Batyn SZ. [2016] Mortality from respiratory diseases in 2014-2015 and ways of its reduction. Pulmonology, 26(4):389-397.

[2] Bystritskaya EV, Bilichenko TN. [2017] Analysis of pneumonia morbidity among adult and child population of the Russian Federation within 2010-2014. Pulmonology, 27(2):173-178.

[3] Chuchalin AG. [2016] Pneumonia: a challenging problem of the XXI century medicine. Therapeutic archive, 88(3):4-12.

[4] Rachina SA, Dekhnich NN, et al. [2016] Estimation of community-acquired pneumonia severity in real clinical practice in combined hospitals of the Russian Federation. Pulmonology, 26(5):521-528.

[5] Chuchalin AG. [2015] Chronic pneumonia. Therapeutic archive, 87(3):4-9.

[6] Bobylev AA, Rachina SA, Avdeev SN, Dekhnich NN. [2016] Clinical significance of C-reactive protein detection in the diagnosis of community-acquired pneumonia. Clinical pharmacology and therapy, 25(2):32-42

[7] Chuchalin AG, Sinopalnikov AI, et al. [2006] Community-acquired pneumonia in adults: practical guidelines for the diagnosis, treatment and prophylaxis. Clinical microbiology and antibacterial chemotherapy, 8(1):54-86.

[8] Kovalchuk LV, Gankovskaya LV, Meshkova RYa. [2011] Clinical immunology and allergiology with the basics of general immunopathology. GEOTAR-Media, Moscow, 640.

[9] Kozlov VA, Borisov AG, Smirnova SV, Savchenko AA. [2009] Practical aspects of immune disorders diagnosis and treatment. Science, Novosibirsk, 274.

[10] Yarilin AA. [2010] Immunology: textbook. GEOTAR-Media, 727.

[11] Gavriliuk EV, Konoplya AI, Karaulov AV. [2016] The role of immune alterations in the pathogenesis of arterial hypertension. Immunology, 37(1):29-34.

[12] Geltser BI, Kim AP, Kotelnikov VN, Makarov AB. [2015] Immune response characteristics in patients with community-acquired pneumonia and endogenous intoxication of different severity. Cytokines and inflammation, 14(3):35-41.

[13] Loktionov AL, Konoplya AI, Evsegneyeva IV. [2013] Acute pancreatitis as clinical-mmunological problem (literature review), Physiology and pathology of the immune system. Immune pharmogenetics, 17(11):3-17.

[14] Loktionov AL, Konoplya AI, Lunev MA, Karaulov AV. [2015] Immune and oxidative disorders in the pathogenesis of inflammatory periodontal diseases. Immunology, 36(5): 319-328.

[15] Mirkhaydarov AM, Farkhutdinov UR, Farkhutdinov RR. [2016] Immunovenin efficacy in treatment of free-radical oxidation and immune status in patients with community-acquired pneumonia. Pulmonology, 26(2):190-195.

[16] Sukovatykh BS, Konoplya AI, Blinkov Yu. [2015] Mechanisms of abdominal sepsis development. Annals of surgery, 2:5-10.

[17] Chuchalin AG, Sinopalnikov AI, Kozlov RS, Tyurin IE, Rachina SA. [2010] Community-acquired pneumonia in adults: practical guidelines for the diagnosis, treatment and prophylaxis. Manual for physicians, 106.

[18] American Thoracic Society, Infectious Diseases Society of America. [2005] Guidelines for the management of adults with hospital-acquired, ventilator-associated, and healthcare-associated pneumonia. Am J Respir Crit Care Med, 171(4): 388-416.

[19] Chroneou A, Zias N, Beamis JF, Craven DE. [2007] Healthcare- associated pneumonia: principles and emerging concepts on management. Exp Opin Pharmacoter, 8(18):3117-3131.

[20] Medvedev AN, Mayanskiy AN, Chalenko VV. [1991] The way to study phagocytosis absorption phase. Laboratory science, 2:19-20.

[21] Shcherbakov VI. [1989] The use of NBT test to estimate neutrophil sensitivity to stimulants. Laboratory science, 1:30-33.

[22] Gorozhanskaya EG. [2010] Free-radical oxidation and antioxidant defense mechanisms in a normal cell and in tumor diseases (lecture). Clinical laboratory diagnostics, 6:28-44.

[23] Sviridova SP, Sytov AV, Kashiya ShR, Sotnikov AV. [2014] Nitric oxide part in the pathogenesis of sepsis-induced multiple organ failure. Annals of intensive therapy, 2:8-17.

[24] Gladkikh RA, Molochniy VP, Polesko IV. [2016] Neopterin as a modern inflammatory marker, Children's infections, 15(2):19-24.

[25] Ivanov AN, Puchinyan DM, Norkin IA. [2015] Endothelium barrier function, mechanisms of its regulation and impairment. Successes of physiological sciences, 46(2):72-96.

[26] Salomatina LV. [2014] Clinical and diagnostic significance of C-reactive protein detection to assess chronic systemic inflammation. Russian Immunology Journal, 8(17)(3):596-599.

[27] Yarilin AA. [2010] Immunology: textbook. GEOTAR-Media, 727.

[28] Spits H, Artis D, et al. [2013] Innate lymphoid cells, aproposal for a uniform nomenclature. Nat Rev Immunol, 13(2):145-149.

[29] Budyakov SV, Konoplya NA, Konoplya AI, et al. [2010] Clinical experience of immunomodulatory agents and antioxidants administration in maxillary sinusitis complex treatment. Guidelines for otolaryngologists, general practitioners, pediatricians. Clinical immunologists, pharmacologists and clinical interns. Belgorod: Publisher BelSU, 40.

[30] Konoplya AI, Gavrilyuk VP, et al. [2015] Clinical experience in combined administration of immunomodulatory agents, antioxidants and membrane protectors in clinical practice. Kursk city printing house, 160.

ARTICLE

PSYCHONEUROLOGICAL DISORDERS IN CHILDREN WITH ATOPIC DERMATITIS

Olesya Evgenevna Kuzina[1], Timur Sergeevich Petrenko[2]*

[1]*Ural State Medical University, Ekaterinburg, Russian federation, RUSSIA*

[2]*Ural Federal University, Ekaterinburg, Russian federation, RUSSIA*

ISSN 0976-3104

ABSTRACT

Background: *Atopic dermatitis (ATD) is a chronic relapsing skin disease. It is characterized by itchy and eczematogenic lesions (pruritus, erythema, pemphigus, papulation, exudation, cortex). Over the past three decades, the incidence of ATD has been steadily increasing. Atopic dermatitis is a common disease in pediatric dermatological practice.* ***Methods:*** *The study is included 217 children of both sexes in the age from 6 to 12 years old. The main group is consisted of 147 children (74 boys and 73 girls), the average age was 8.7 ± 1.88 years with a diagnosis of ATD determined earlier. The assessment was carried out by a dermatologist with SCORAD scale. A comparison of the shares was used for the analysis of qualitative features, (chi-square test with Yeats correction for continuity).* ***Results:*** *Neurosis-like disorders in the form of thikoid hyperkinesis, stuttering, enuresis, encopresis, sleep and appetite disorders among children in the main group were noted in 80.6% of cases (n = 62), among children in the control group - in 13.3% of cases (n = thirty). In more than half of cases, children with ATD had dissominal disorders (66.7%, n = 62).* ***Conclusions:*** *Neuropsychiatric symptoms in children with atopic dermatitis are due to the action of exogenous organic factors pathogenic for the central nervous system in the early stages of ontogenesis. Sensory and motor deprivation of a child at an early age (up to 3 years), which inevitably occurs due to the manifestation of somatic suffering, aggravates the formation of neuropsychological deficiency and the structuring of residual cerebroorganic symptoms.*

KEY WORDS
Children; atopic dermatitis; mental disorders; neuropsychology

INTRODUCTION

Over the past three decades, the incidence of ATD has been steadily increasing [1]. The proportion of ATD among allergic diseases in the pediatric population is up to 75%. The disease is detected in people of both sexes and in different age groups. Girls get sick 1.5 times more often than boys. In 70% of cases, ATD is debuting in the first year of life. Moreover, half of the children subsequently form an “atopic march” - the addition of hay fever, allergic rhinitis, and often bronchial asthma [2]. The disease is detected in people of both sexes and in different age groups. Girls get sick 1.5 times more often than boys. In 70% of cases, ATD is debuting in the first year of life. Moreover, half of the children subsequently form an “atopic march” - the addition of hay fever, allergic rhinitis, and often bronchial asthma [2]. Common associated problems in this case are: school maladaptation, attention deficit hyperactivity disorder, neurotic disorders. As adults, such patients are prone to anxiety and depressive disorders, have frequent conflicts in the family, and abuse psychoactive substances.

A large number of scientists believe that stress in infancy can instigate damage to the neuroendocrine system, thus laying the patho-genetic basis for the autoimmune process [2]. Subsequently, the functioning of the hypothalamic-pituitary-adrenal axis, the immune-skin system, and central neuro-mediator processes is disrupted [3]. It explains the frequent occurrence of anxiety-depressive syndromes in patients with ATD.
Proponents of the psychoanalytic concept associate the symptoms of the disease with the development of specific neurotic personality traits [2]. The obsessive itching feeling and the desire to scratch are a reflection of the unconscious indefatigable feeling of resentment against the mother for the lack of warmth and love at a very young age [4].

Received: 1 Dec 2019
Accepted: 10 Mar 2020
Published: 12 Apr 2020

Modern neuropsychological studies reveal in children with ATD the underdevelopment of the energy block and the weakness of the activating brain system [5]. Such violations can be explained by diffuse organic damage to the central nervous system (CNS) (with predominant localization in the mid-stem structures) in the early stages of ontogenesis. Moreover, the limitation of tactile contact with the mother in connection with the manifestation of symptoms of ATD aggravates the clinic of the emerging neuropsychiatric disorders [6].

The aim of the study was to establish the clinical and patho-genetic patterns of the development of mental disorders in children with ATD.

MATERIALS AND METHODS

Subjects: The study was conducted at the clinical base of the Department of Psychiatry of the Ural State Medical University in the period from 2016 to 2018 years (Protocol of approval by the local ethics committee of UMMU No. 6 dated 06.24.2016). The study included 217 children of both sexes in the age from 6 to 12 years, attending kindergartens and elementary grades of secondary schools. The intelligence level was accorded to the Wexler test, it was not lower than average (IPR> 90 points).

***Corresponding Author**
Email:
olesya-kuzina-96@mail.ru
Tel.: +79122760819

IIOAB JOURNAL
ISSN: 0976-3104

Inclusion exclusion criteria: The main group consisted of 147 children (74 boys and 73 girls), the average age of which was 8.7 ± 1.88 years with a diagnosis of ATD determined earlier (at least one year) according to the ICD-10 (L20) criteria, without severe somatic or mental pathology. Given the comparative age approach in the study, three age subgroups were identified: 6–7 years (n = 62), 8–10 years (n = 55), and 11–12 years (n = 30).

Clinical examinations: The severity of the clinical manifestations of ATD at the time of examination among the children of the main group ranged from mild to severe. The assessment was carried out by a dermatologist on the SCORAD scale [7]. A mild degree was detected in 53.1% of the children of the main group (n = 147), the average value on the SCORAD scale was 16.7 ± 9.8 (n = 78). A moderate degree of clinical manifestations was noted in 33.3% of children with ATD (n = 147), the average SCORAD value was 33.8 ± 10.2 (n = 49). A severe clinic was noted in 13.6% of the children of the main group (n = 147), the average SCORAD value was 62.1 ± 13.8 (n = 20). In 43 children of the main group, concomitant bronchial asthma was detected; 34 children have gastroesophageal reflux disease. The presence of hereditary burden due to atopic diseases by close relatives was noted in 34.0% of cases (n = 147). Among children with a hereditary disease, children of the older age category with a stable mild or moderate clinic prevailed. The control group consisted of 90 children (45 boys and 45 girls) with indicators of relative somatic health. The average age of children in this group was 8.7 ± 1.94 years. In each age category, there were 30 children.

The main research methods were clinical-anamnestic and clinical-psychopathological. To establish the clinical regularities of the course of mental disorders in ATD, an approach was used based on the periodization of the stages of the neuropsychic response of children [8]. An in-depth analysis of all pathogenic factors that influence on the occurrence, clinical dynamics of psychopathological disorders were associated with AT, depending on the age stages of the neuropsychic response. The clinical method was accompanied by an assessment of the mental and neurological status among all children of the main and control groups according to the generally accepted pattern [9]. The psychopathological method was supplemented by a questioning of parents using a questionnaire to assess the neuropsychic sphere of the child, proposed by N.N. Zavadenko [10]. Most of the children of the main group (n = 105) underwent a neuropsychological study using the adapted neuropsychological study [11], shortened in comparison with the generally accepted method A.R. Luria. An objective study was carried out according to the scheme, which included 67 samples related to 14 studied functions: thinking, speech, memory, praxis, gnosis, coordination. The interpretation of the results of a neuropsychological examination was based on the identification of disorders, the determination of topical lesions and related dysfunctions of the brain systems.

Statistical analysis: Statistical processing of the obtained data was carried out on a personal computer running the Windows 10 operating system using the Statistica 12 program. For the analysis of qualitative features, a comparison of the shares was used (chi-square test with Yeats correction for continuity). The differences were regarded as significant at a confidence level of $p < 0.05$ [12].

Ethical statement: The work was carried out with case histories of patients, who were taken from the archive, personal data of patients. The case histories were not disclosed.

RESULTS

The influence of pathogenic factors: In the course of the clinical and anamnestic study, pathogenic factors were identified. Pathogenic factors were contributed to the formation of mental disorders that acted at the very early stages of development. Thus, in the main group, signs of pathology of pregnancy of the mother were significantly more often compared with the control group in the form of: a burdened obstetric and gynecological history (50.3%, n = 147); threats of termination of pregnancy at different periods (40.8%, n = 147); development of intrauterine hypoxia (55.8%, n = 147); transferred during pregnancy or chronic infectious diseases (43.5%, n = 147); consumption of nicotine or alcohol at different stages of pregnancy (26.5%, n = 147).

The frequency of birth pathology in the studied groups had significant differences. Premature (less than 37 weeks) or postponed (over 42 weeks) pregnancy in the main group occurred in 40.1% of cases (n = 147), in the control group - 23.3% (n = 90). Operational resolution of childbirth (emergency or planned) in mothers of children of the main group took place in 29.2% of cases (n = 147), in the control - in 12.2% of cases (n = 90). Asphyxia in childbirth was observed in 55.8% of children with ATD (n = 147) and 3.3% of healthy children (n = 90). The diagnosis of perinatal damage to the central nervous system (PCNS) was established in 42.2% of cases among children of the main group (n = 147) and in 8.9% of cases among children of the control group (n = 90).

Analysis of the manifestation of the clinical manifestations of ATD in children of the main group shows that in most cases the onset of the disease occurred in 1–2 years of the child's life (68.0%, n = 147). Less commonly, symptoms developed between 2 and 5 years (21.8%, n = 147). In rare cases, clinical manifestations began after 6 years (10.2%, n = 147). In almost half the cases, parents attribute the onset of the disease to a traumatic factor - fear, emotional stress, etc. An examination of the family's psychological climate, types of upbringing, and social conditions of living did not reveal significant differences among the children of the main and control groups.

IIOAB JOURNAL
ISSN: 0976-3104

According to the anamnesis and medical records, an organic neuropathy syndrome was detected at the age of 1 year, which was represented by increased excitability with prolonged crying, motor anxiety with hypertonicity and tremor, autonomic dysfunction in the form of hyperhidrosis, sub febrile conditions, sleep disturbance and wakefulness. The prevalence of the described phenomena among children of the main group was 82.3% (n = 147), among children in the control group -30.0% (n = 90). 30.6% of children with ATD (n = 147) had a history of convulsive paroxysms up to 1 year old.

The study of possible pathogenic factors for the central nervous system in the period up to 3 years revealed a difference between the groups in the frequency of colds. Thus, frequent colds (more than 4 times per year) among children with ATD were noted in 66.6% of cases (n = 147), and among children in the control group - in 27.8% of cases (n = 90).

The effect of artificial feeding: Some researchers associate the pathogenesis of ATD with early sensitization of the child's body resulting from artificial feeding [13]. In the present study, no significant differences were found between the groups in the initial type of feeding. However, the period of breastfeeding in most children of the main group was not exceed 4 months (75.5%, n = 147). Among children in the control group, a similar transition to artificial feeding was noted only in 32.2% of cases (n = 90). There were also no differences between the groups of mothers of children who used allergenic products during the period of active breastfeeding.

Speech and motor skills: We studied the development of speech and motor skills during the first age crisis (3-4 years), when the somato vegetative stage ends and the psychomotor begins. Speech and psychomotor disturbances obviously reflect damage to brain structures in the early stages of its development. The delay in speech development by the age of 4 years was observed in children of the main group in 60.5% of cases (n = 147), in the control group - in 17.8% of cases (n = 90). The delay in the formation of motor skills in the main group was noted in 62.6% of cases (n = 147), in the control group - in 8.9% of cases (n = 90).

The formation of neurosis-like disorders is depending on the age period. Clinical and psychopathological study of children in various age categories allows us to identify the typology and dynamics of neuropsychiatric disorders in children with ATD. The seventh and eighth years of a child's life corresponds to the second critical age period, when the affective (7-12 years) is superimposed on the psychomotor stage of development (3–10 years). This stage is characterized by decompensation of residual organic cerebral insufficiency in the form of formalized psycho-vegetative disorders, manifestation of psychomotor disorders, and the onset of the formation of neurosis-like disorders. In the next age category of 8–10 years, there is compensation for psycho-vegetative disorders that have begun earlier, a clinic of psychomotor disorders is revealed, and neurosis-like syndromes are formed. At the age of 11–12 years, the following critical period arises, associated with the end of the affective and the beginning of the emotionally-ideational stage of development, the formation of self-awareness. This period is characterized by decompensation of current cerebro-organic disorders that significantly affect the formation of personality traits. Accordingly, during this period patho-character reactions, affective vibrations, and psychopathic disorders are actively progressing [14].

Among children of the age category 6–7 years, manifestations of cerebral growth in the form of persistent headache with nausea and nosebleeds, meteorological dependence, irritable weakness and vestibule-vegetative disorders were detected in 88.7% of cases among children of the main group (n = 62), among children of the control group - in 30.0% of cases (n = 30). Neurosis-like disorders in the form of thikoid hyperkinesis, stuttering, enuresis, encopresis, sleep and appetite disorders among children in the main group were noted in 80.6% of cases (n = 62), among children in the control group - in 13.3% of cases (n = thirty). In more than half of cases, children with ATD had dissominal disorders (66.7%, n = 62). 23 children of the main group of this age category (n = 62) showed signs of attention deficit hyperactivity disorder (ADHD) that meets the ICD-10 criteria (F90).

In the age category of 8–10 years, 69.1% of children with ATD (n = 55) retain cerebrosthenic phenomena, which are milder in comparison with the previous age category, but with more frequent manifestations of emotional lability. Among children in the control group, cerebrosthenic disorders were noted in 20.0% of cases (n = 30). Also, neurosis-like syndromes were noticeably less common in children of this age: 65.5% of cases (n = 55) in children of the main group, 10.0% of cases in children of the control group (n = 30). In 41.8% of children with ATD at the age of 8–10 years (n = 55), neurotic reactions of the "avoidant type" to generalized skin manifestations were revealed. At 15 children of the main group (n = 55) parents noted hysterical failure reactions in predisposing situations; in 11 children with ATD (n = 55), anxiety-phobic and depressive states were noted; 18 children in this group (n = 55) showed signs of ADHD. No similar phenomena were detected among children of the control group.

In children in the age group of 11–12 years, cerebral phenomena occurred in 33.3% of cases in the main group (n = 30) and in 13.3% of cases in the control group (n = 30). In such children, affectively excitable character traits and dysphoric paroxysms were revealed. More than half (56.7%) of children of this age with ATD (n = 30) had neurotic reactions in the form of anxiety-phobic, anxious-suspicious or depressive short-term (up to two weeks) conditions. Impaired disturbances in the form of stuttering, enuresis, and dysomnia were detected in 56.7% of children in the main group (n = 30) and 13.3% in the control group (n = 30). Adolescent ADHD was found in 12 children of the main group of the 11–12 year old age group (n = 30). Patho

IIOAB JOURNAL
ISSN: 0976-3104

characterological reactions were observed in 56.7% of children with ATD at the age of 11–12 years (n = 30) were represented by reactions of rejection, opposition, compensation and hyper compensation, emancipation.

An analysis of the influence of the psychological state on the clinical manifestations of ATD revealed an increase in the clinical manifestations of the disease against the background of stress of various origins in 43 children of the main group (n = 147). Usually, such an exacerbation was of a short-term nature — it was not exceed two weeks.

DISCUSSION

As a result of a comparative study, clinical features were analyzed and patterns of development of psycho-neurological disorders in children with ATD were revealed. The pathological course of pregnancy, detected in most children with ATD (82.3%, n = 147), creates conditions for increased vulnerability of the central nervous system of the fetus. Impaired development of the fetus (40.1% of children with ATD, n = 147) leads to immune-endocrine disorders, contributing to the development of atopic processes. Diffuse organic damage to the brain contributes to asphyxia and PCA, detected in childbirth in children with ATD (42.2%, n = 147). All these factors were decisive in the development of subsequent psychopathological and neurological manifestations of residual-organic genesis and corresponding to the stages of neuropsychic response. The manifestation of the disease, which occurred mainly in the first two years of life in most cases in children with ATD, was accompanied by symptoms of organic neuropathy under the age of 1 year. By age 3-4 years, many of these children experienced a delay in speech and psychomotor development. Decompensation of residual-organic damage to the central nervous system at the age of 6–7 years was manifested by powerful cerebro-stenic symptoms. Disturbances characteristic of the psychomotor stage of the neuropsychic response (ADHD, tics, stuttering) were manifested. Compensation of cerebral age 8–10 years old in most children with ATD was accompanied by active neurosis-like symptoms in the form of affective reactions, neurotic states associated with the appearance of the skin [5]. At the age of 11–12 years, more than half of children with ATD have joined the existing clinic patho-character reactions with affective-excitable traits and dysphoroid-like paroxysms. The most pronounced neuropsychological disorders in children with ATD were found in the work of the first (energy) block of the brain, which was manifested by a lack of neuro dynamic regulation. The work of the second and third functional blocks in such children is characterized by stiffness and underdevelopment of alternative algorithms, which is due to the weak development of the system of intra- and interhemispheric connections. In our opinion, an additional factor in the development of neuropsychological deficiency is the deprivation of sensory and kinesthetic sensations resulting from the development of skin disease.

Psychological factors of a family nature had a limited impact in the study group. Apparently, the effect of such factors is significant only in the presence of an initial organic central nervous system inferiority.

The results of the clinical and anamnestic study revealed pathogenic factors that predetermined the clinical dynamics of psychopathological and neurological disorders. Those disorders correspond to the dynamics of residual-organic cerebral insufficiency, with a characteristic change in the leading symptoms in accordance with the stages of the neuropsychic response.

In the article by Professor Retyunsky, “Neuropsychiatric Disorders in Children with Atopic Dermatitis,” the neuropsychiatric module of pathogenesis explains the occurrence of ATD by dysfunction of autonomic centers due to early perinatal damage to the central nervous system [5]. Our study confirms these findings. Neuropsychiatric build-up in children with ATD is due to the action of exogenous organic factors pathogenic for the central nervous system in the early stages of ontogeny. Sensory and motor deprivation of a child at an early age (up to 3 years), which inevitably occurs due to the manifestation of somatic suffering, aggravates the formation of neuropsychological deficiency and the structuring of residual cerebroorganic symptoms. Jonathan I. Silverver in his research says that children with ATD are at higher risk for neuropsychiatric disorders, including speech disorders, depression, hyperactivity and seizures. Our article also confirms this statement [15].

CONCLUSION

An analysis of the clinical patterns of the development of mental disorders in children with ATD opens up prospects for the discovery of common patho-genetic mechanisms in the development of neuropsychiatric, somato-vegetative and neuro-immune disorders in ATD. This would allow to develop a set of sound medical, rehabilitation and preventive measures to combat ATD and related disorders. We offer an effective biopsychosocial approach to the treatment of children with ATD, which includes comprehensive psycho pharmacotherapy, neuropsychiatric correction, and social work. Since the altered brain is the biological basis of the pathophysiological mechanisms of ATD, the complex of psycho pharmacotherapy includes nootropic, dehydration, vascular therapy, which is taken in courses of 30 days and repeated up to 4 times a year for 3 years. If the disease is accompanied by tics, stuttering, enuresis, epileptic form activity, anti colvantants should be included in the therapy. Efficiency criteria will be the normalization of the general condition of the child, the reduction in the time to achieve remission of skin processes.

IIOAB JOURNAL
ISSN: 0976-3104

CONFLICT OF INTEREST

The authors declare no competing interests in relation to the work.

ACKNOWLEDGEMENTS

The authors sincerely thank the Municipal Children's City Polyclinic No. 13 for providing these patient histories.

FINANCIAL DISCLOSURE

The author of the article is a student. This work is not funded by any funding agency.

REFERENCES

[1] Revyakina VA, Smirnov GI. [2004] Scientific and practical program atopic dermatitis and skin infections in children: diagnosis, treatment and prevention, Questions of modern pediatrics, 5(3):30–32.
[2] Jafferany M. [2007] Psycho dermatology: A Guide to Understanding Common Psycho cutaneous Disorders Prim Care Companion, J Clin Psychiatry, 9(3):203–213.
[3] Afsar F, Isleten F, Sonmez N. [2010] Children with atopic dermatitis do not have more anxiety or different cortisol levels compared with normal children, Journal of Cutaneous Medicine, 14(1):13-8.
[4] Manzoni A, et al. [2013] Assessing depression and anxiety in the caregivers of pediatric patients with chronic skin disorders, An Bras Dermatol, 88(6):894-899.
[5] Retyunsky KY, Sokolova IV. [2011] Neuropsychiatric disorders in children with atopic dermatitis, Scientific reports of Belgorod State University: Medicine. Pharmacy, 4(13):30–34.
[6] Yusupova LV, Retyunsky KY. [2013] Non-psychotic psychiatric disorders of residual-organic genesis in young children who suffered a perinatal lesion of the central nervous system, Practical Medicine, 1(66):176–181.
[7] Kamasheva GR, Khakimova RF, Valiullina SA. [2010] Methods for assessing the severity of atopic dermatitis in young children, Zemsky Doctor, 19(6):32–34.
[8] Kovalev VV. [1995] Child Psychiatry: A Guide for Physicians, Moscow: Publishing House Medicine, RU.
[9] Badalyan LO, Zhurba LT. [1998] A Guide to Pediatric Neurology, Moscow: Health Publishing House, RU.
[10] Zavadenko NN. [2005] Hyperactivity and attention deficit in childhood: a study guide for students. Higher textbook, Moscow: Yurayt Publishing House, RU.
[11] Simernitskaya EG. [1991] Neuropsychological technique of express diagnostics "Luria-90", Moscow: Knowledge Publishing House, RU.
[12] Glanz S. [1999] Biomedical statistics, Moscow: Practice Publishing House, RU.
[13] Toropova NP, Sorokina KN, Lepeshkova TS. [2014] Atopic dermatitis in children and adolescents-the evolution of views on pathogenesis and approaches to therapy, Russian Journal of Skin and Sexually Transmitted Diseases, 6(17)50–59.
[14] Sukhareva GE. [2004] Lectures on child psychiatry, Moscow: Education Publishing House, RU.
[15] Jonathan I. [2017] Selected comorbidities of atopic dermatitis: Atopy, neuropsychiatric and musculoskeletal disorders, Clinics in Dermatology, 35(4):360-366.

ARTICLE

DYNAMIC SECURITY ASSESSMENT OF INTERCONNECTED POWER SYSTEMS

Badr M. Alshammari*, Tawfik Guesmi
College of Engineering, University of Ha'il, SAUDI ARABIA

ISSN 0976-3104

ABSTRACT

Modern power systems continue to grow in size and complexity due to the high demand for electricity. Thus, dynamic security assessment (DSA) is becoming a necessary requirement in the system operation. The critical clearing time (CCT) is a key issue for DSA. Nonlinear time domain simulation (NTDS) is the most accurate method for computing CCT. Unfortunately, DSA is often confronted by the high nonlinearity of interconnected power networks. Thus, NTDS-based DSA is considered time consuming and needs heavy computational effort. In order to avoid these drawbacks, this paper deals with a new technique for online DSA of interconnected power system. Such technique is developed in two steps. Firstly, NTDS is used to compute CCTs for various loading conditions. Then, adaptive network based fuzzy inference systems (ANFIS) is used to establish the relationship between the operating conditions and the corresponding CCTs. The approach effectiveness is validated on two multimachine power systems under severe fault disturbances.

KEY WORDS
Power system faults; Power system stability; Nonlinear network analysis; Fuzzy neural networks.

INTRODUCTION

Due to the increasing demand and requirement for electric power, dynamic stability is having a significant importance in the operation of power networks. Stability is the ability of the power system to return to a normal operating state when subjected to disturbances [1-2], such as, short-circuits, loss of a tie between lines or sudden variation of operating conditions. Due to the occurrence of faults one or more generators can be seriously disturbed causing an unbalance between production and demand. If a fault persists and is not removed within a predefined period of time, it may cause serious equipment damage and may result in loss of power. To deal with this problem, dynamic security assessment (DSA) based on stability studies has become one of the essential tools for planning, designing and improving electrical networks.

In recent years, several research works have focused on the stability analysis of power systems [3-10]. Critical clearing time (CCT) is one of the most important parameters that measure the stability limits of the power network against disturbances. It is defined as the longest fault clearing time which can be allowed before the generators losses the synchronism [4]. Several methods have been proposed in the literature in order to calculate the CCT [10-15]. These methods differ from each other in the assumptions adopted and the modeling techniques. They can be classified into four groups which are (i) energy based methods [13-15], (ii) numerical integration methods [16-17], (iii) stochastic methods [18-19] and (iv) hybrid techniques [20]. A direct energy method based on the Lyapunov energy function was proposed in [15] to study the transient stability of the power network system. The energy based approaches were used to determine the stability limits without resorting to resolution of the state space differential equations of the system which makes them fast. However, the main drawback of such approaches is the selection of the optimum Lyapunov function which may affect the accuracy of the stability assessment. Long Vu and Turitsyn [5] presented a semi definite programming based technique for the construction of the Lyapunov function used for the DSA problem.

Received: 12 Mar 2020
Accepted: 20 Apr 2020
Published: 24 Apr 2020

Numerical integration consists in finding a mathematical model capable of representing the system dynamics during three important phases that are before, during and after disturbance. Differential equations are resolved in the time domain using numerical integration methods such as Euler method and Runge-Kutta technique [21]. Then, simulation results can be directly interpreted by users, and the mechanisms of instability can be examined in detail. In recent years, various research studies have demonstrated that techniques based on the nonlinear time domain simulation (NTDS) provide the most accurate CCT [6]. NTDS-based techniques have been implemented by using the numerical integration of the nonlinear state space differential equations of the power network. Unfortunately, these techniques cannot be applicable for the online assessment of the system dynamics and CCT calculation because they are time consuming and need heavy computational effort [6].

To overcome these difficulties, novel intelligent techniques based on artificial neural network (ANN) and fuzzy logic have been proposed for predicting CCT and assessing power system dynamics [11]. Approaches based on ANNs and fuzzy logic have the ability to learn and model complex and nonlinear relationships. Moreover, they don't impose any limitations on the number of inputs and outputs. A neural-based approach has been proposed for online CCT estimation [6]. The approach was based on a feedforward neural network trained off-line using an historical database. Other algorithm based on multi-layer feedforward neural network has been proposed in [8] for real-time stability assessment. In [9], a transient stability model based on back propagation neural network has been suggested to assess transient stability. The load pattern has been chosen as ANN input and CCT has been considered as output. To calculate CCTs necessary for the training set, the multimachine system has been converted into single

***Corresponding Author**
Email:
bms.alshammari@uoh.edu.sa
Tel.: +966-506066644

IIOAB JOURNAL
ISSN: 0976-3104

machine infinite bus. Sulistiawati et al. [10] have presented a new technique based artificial intelligence for CCT prediction. Calculation of the CCT has been done using the critical trajectory method.

Within this context, this study presents a new technique for online assessment and enhancement of interconnected power system stability. To do so, this online assessment method is based on two steps. First, CCT are computed for various loading conditions using Runge-Kutta method and time domain simulation. The second step is based on adaptive network-based fuzzy inference system (ANFIS) training with the collected input-output data pairs which are stocked in the first step. The input data are operating conditions and the outputs are CCTs. In this study, operating conditions are described by load real and reactive powers. The proposed approach is tested on a multimachine power system under different loading conditions. Results show that the proposed method works effectively over a wide range of arbitrary operating conditions and can be applicable for real-time DSA.

MATERIALS AND METHODS

Machine classical model

In this paper, synchronous machines are described by the third-order model [5, 21]. Thus, each machine is modeled by two motion equations and the generator internal voltage equation.

$$s\delta_i = \omega_b(\omega_i - 1) \quad (1)$$

$$s\omega_i = (P_{mi} - P_{ei} - D_i(\omega_i - 1))/M_i \quad (2)$$

$$sE'_{qi} = \left(E_{fdi} - (x_{di} - x'_{di})i_{di} - E'_{qi}\right)/T'_{do} \quad (3)$$

The electrical power P_e can be expressed by the d-axis and q-axis components of the terminal voltage V_t and the armature current *i* as follows [21].

$$P_{ei} = v_{di}i_{di} + v_{qi}i_{qi} \quad (4)$$

where,

$$v_{di} = x_{qi}i_q \quad (5)$$

$$v_{qi} = E'_{qi} - x'_{di}i_{di} \quad (6)$$

$$V_{ti}^2 = v_d^2 + v_q^2 \quad (7)$$

Using equations (4)–(6), the electrical power can be written as.

$$P_{ei} = E'_{qi}i_{qi} + \left(x_{qi} - x'_{di}\right)i_d i_q \quad (8)$$

CCT computation using numerical integration

Let consider t_a and t_c the application and clearing times of the disturbance. The behavior of the faulted system is studied in the time interval [t_a,t_c]. On the other hand, the behavior of the post-fault system is studied between the fault clearance time and simulation end time, t_f. If t_a = 0, the critical clearing time (CCT) is the maximum value of t_c for which the system remains stable. In this study, the CCT is determined using Runge-Kutta method.

Step 1: Enter system data
Step 2: Iteration = 0.
Step 3: Load flow calculation for the pre-fault system
Step 4: Computation of the bus admittance matrices for the pre-fault (Y1), during fault (Y2) and post-fault cases.
Step 5: Iteration = iteration + 1.
Step 6: Integration of the faulted system between ta and t_c.
Step 7: Integration of the post-fault system between t_c and t_f.
Step 8: Visualization of the rotor angle curves.
Step 9: Decision about the stability of the system from the rotor angle curves.
Step 10: If the system is stable, increase t_c and got to step 5. Otherwise, go to step 10.
Step 11: If iteration > 1, CCT = t_c. Otherwise, decrease t_c and go to step 12.
Step 12: iteration = 0 and go to step 5.

Numerical integration based on the Runge-Kutta method is the most accurate approach for determining the CCT [6]. Unfortunately, it presents many difficulties for the on-line applications due to its excessive computation time.

IIOAB JOURNAL
ISSN: 0976-3104

Implementation of the ANFIS based approach

ANFIS was originally suggested in [22], where the ANFIS architecture was presented to model nonlinear functions, identify nonlinear components on-linely in a control system and predict a chaotic time series. As in [22], this ANFIS has five layers. A description of each layer is presented in [23].

Selection of initial number of membership functions is an important step in the ANFIS application. In [23], the authors have determined this number by trial and error. They demonstrated that this method was not effective because it is based on a grid partition and it causes an explosion of the number of rules when the inputs number is large. So, they have proposed another method based on a clustering algorithm. The objective of clustering is to generate a concise representation of a system's behaviour by dividing the data space into clusters. Several clustering methods are used in literature [23]. In this paper, a procedure based on subtractive clustering algorithm is used to generate the initial fuzzy inference system (FIS) structure. This non-iterative algorithm is based on a density measure at data point in the feature space, as follows.

Step 1: Consider a set of *n* data points $\{X_1, X_2, \cdots, X_n\}$. The density measure at point X_i is described by the following equation.

$$D_i = \sum_{j=1}^{n} \exp\left(-\frac{\left\| X_i - X_j \right\|^2}{\left(r_a / 2 \right)^2} \right) \tag{9}$$

r_a is a positive constant representing a neighborhood radius.

Step 2: Select the data point X_{C1} having the highest density D_{C1} as the first cluster center. Then, update the density measure of each data point X_i using the following equation. r_b is a positive constant.

$$D_i = D_i - D_{C1} \exp\left(-\frac{\left\| X_i - X_j \right\|^2}{\left(r_a / 2 \right)^2} \right) \tag{10}$$

Step 3: Select the next cluster center and revise the density measure of data points. Repeat this process until a sufficient number of clusters is reached.
In this study, the ANFIS block is employed to establish the relationship between operating conditions and the corresponding CCT. ANFIS block input are load real (P_{Li}) and reactive (Q_{Li}) powers.

RESULTS

To evaluate the effectiveness and robustness of the proposed ANFIS-based DSA, its performance has been examined on the 3-machine 9-bus WSCC (western system coordinating council). The system data and its single line diagram can be found in [1, 24]. The system operating condition for the base case is depicted in Table I.

Table 1: System operating condition for the base case

		P [pu]	*Q* [pu]
Gen	G1	0.72	0.27
	G2	1.63	0.07
	G3	0.85	-0.11
Load	A	1.25	0.50
	B	0.90	0.30
	C	1.00	0.35

Data collection phase

A 6-cycle fault disturbance at bus 5 at the end of line 5–7 is considered. The fault is cleared by tripping the line 5–7 with successful reclosure after 1.0s. In this phase, the CCT is computed using Runge-Kutta method for several operating conditions defined by equations (11) and (12).

$$P_{Li} = \lambda_p P_{L0_i} \tag{11}$$

$$Q_{Li} = \lambda_q Q_{L0_i} \tag{12}$$

where, P_{L0_i} and Q_{L0_i} are the nominal active and reactive loads at the *i*-th bus given in Table I. Coefficients λ_p and λ_q are active and reactive loading factors, respectively. They will be ranged independently, from 0.2 to 1.5, in order to cover several values of the load power factors.

The collected input-output data pairs will be stocked in the training set. Inputs are described by the loading factors and outputs are the corresponding CCTs. In this case, the training set is composed of 200 input-output data pairs.

For example, the CCT is determined for the base case. Fig. 1 shows speed deviations of machines G2 and G3 using the nonlinear time domain simulations. G1 is the reference machine. From Fig. 1, it is clear that the system is stable for fault duration time t_f = 187 ms and it is unstable for t_f = 188 ms. Thus, the CCT is 187 ms.

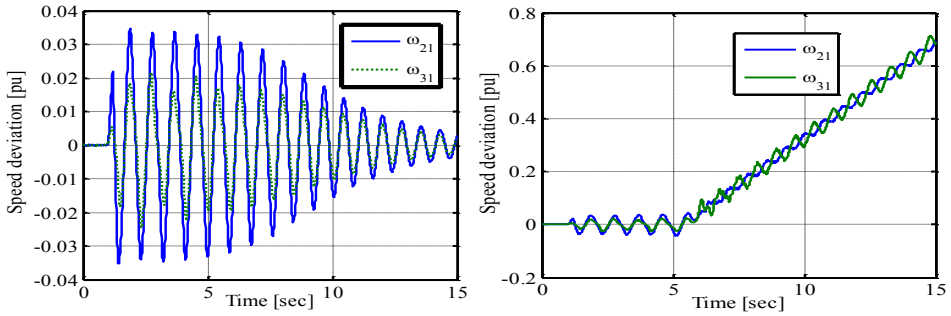

(a) For t_c = 187 ms (b) For t_c = 188 ms

Fig. 1: Change in speed deviations for WSCC system

Fig. 2 shows the electrical power output of the three generators for the same duration faults as previously. It is clear that when the duration fault is more than 187 ms, the system is unstable.

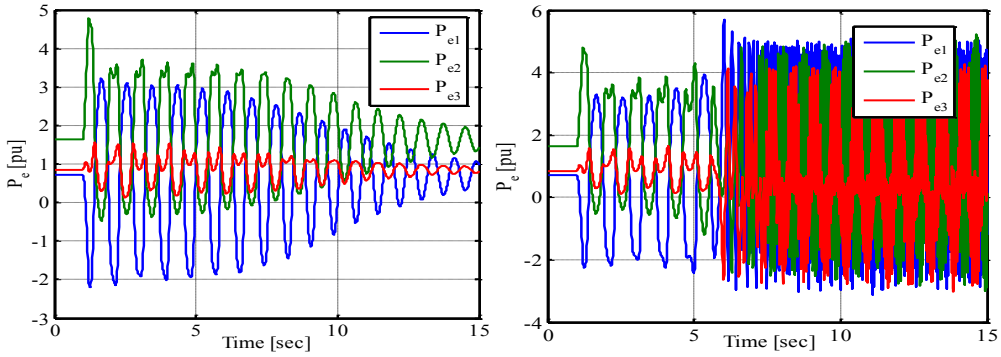

(a) For t_c = 187 ms (b) For t_c = 188 ms

Fig. 2: Variation of the electrical power output for the WSCC system

Training phase

The initial fuzzy inference system (FIS) is trained using ANFIS, to converge to the least possible error between the desired output and the FIS output through the training set. A combination of least-squares and back-propagation gradient descent methods are used. The cluster radius was $r_a = 0.25$.

Fig. 3 depicts a comparison between real training data and checking data obtained for various loading factors. It can be clearly seen that the ANFIS output provides good approximation of the variation of CCTs versus loading conditions.

DISCUSSION

The performance of the proposed online DSA is also confirmed using the New England power system. All system data and the single line diagram are taken from [1,24]. A 6-cycle fault disturbance near bus 29 at the end of the line 26-29 with 20% step increase in mechanical power is applied. The disturbance is removed by tripping the line 26–29 with successful reclosure after 1.0 second. G8 and G9 are the nearest machines to the fault location. Thus, the system DSA can be summarized in studying the dynamic behaviour of these two generators.

The NTDS depicted in Fig. 4 shows an example of computing of the CCT for a loading condition selected randomly from the input set. In this example, $\lambda_p = 1.0266$ and $\lambda_q = 1.2379$. From Fig. 4, it is evident that the corresponding CCT is 172 ms.

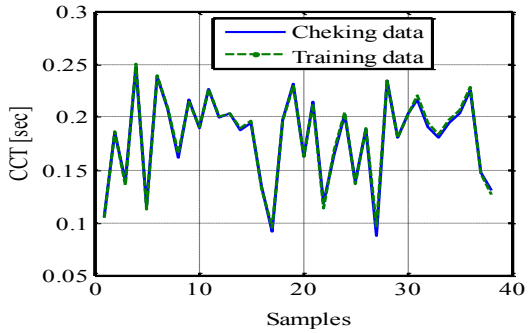

Fig. 3: Checking and training data for WSCC system

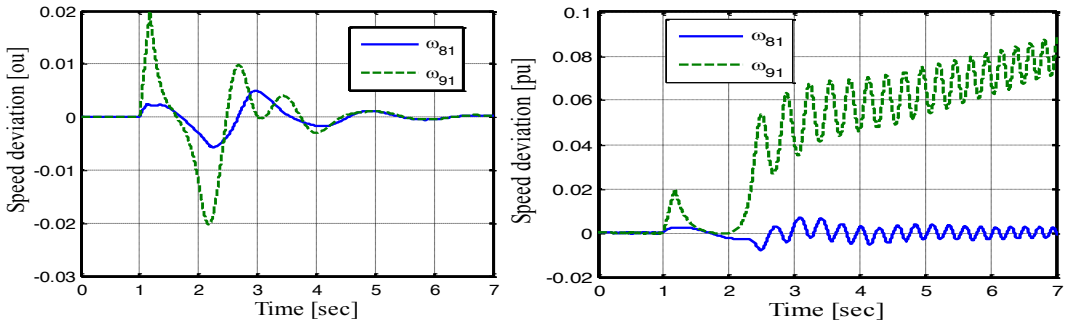

(a) For t_c = 172 ms (b) For t_c = 172 ms

Fig. 4: Variation of the electrical power output for the NE system

Fig. 5 demonstrates the real training data and checking data for various samples of loading conditions. As concluded for WSCC system, the proposed ANFIS-based approach provides accurate values of CCTs. Moreover, Table II shows that the proposed approach is convenient for on-line DSA because of its reduced computation time. In fact, the results presented in Table II show that the CPU time using the proposed method is reduced 8 to 10 times compared to the trajectory-based method presented in [14]. Therefore, it can be concluded that the proposed ANFIS-based method is an accurate technique that can be used for online dynamic security assessment over wide range of operating conditions.

The times reported here were computed using MATLAB R2013a with 64-bit operating system on a PC with an Intel i7-4510U CPU@2.00 GHz.

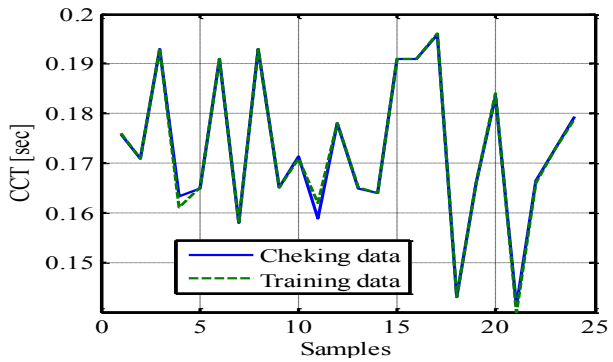

Fig. 5: Checking and training data for NE system

Table. 2: CPU time for the studied techniques

Method	WSCC system	NE system
NTDS	(4 to 8)X0.375 sec	(4 to 8)X0.426 sec
Critical trajectory-based method [14]	0.125-0.156 sec	-
ANFIS-based approach	0.0121 sec	0.0122 sec

IIOAB JOURNAL
ISSN: 0976-3104

CONCLUSION

In order to monitor the security of the power network and specifically to provide an extended visibility of the transmission system to the operator, the online prediction of the CCT is becoming a key issue for the DSA. This paper presents an intelligent technique for online DSA of power networks. This technique can provide an accurate CCT in a rapid and robust way. To do so, CCTs are firstly calculated using NTDS under various loading conditions and severe faults. Then, collected input-output data pairs will be stocked in training set whose inputs are the loading conditions and outputs are the corresponding CCTs. In order to provide real time estimation of CCTs for any loading condition, a neuro-fuzzy based approach is used to establish the relationship between inputs and outputs. Simulation results demonstrated that the proposed method can be applicable for online DSA since it is more than 142 times faster compared to the NTDS method.

CONFLICT OF INTEREST

There is no conflict of interest

ACKNOWLEDGEMENTS

The author would like to thank the Deanship of the Scientific Research of University of Hail, Saudi Arabia for funding and supporting this research project (#161087).

FINANCIAL DISCLOSURE

The research was supported by the Deanship of the Scientific Research of University of Hail, Saudi Arabia (Project N° 161087).

REFERENCES

[1] Guesmi T, Farah A, Hadj Abdallah H, Ouali A. [2018] Robust design of multimachine power system stabilizers based on improved non-dominated sorting genetic algorithms. Electrical Engineering, 100(3):1351-1363.
[2] Choucha A, Chaib L, Arif S. [2017] Robust control design of PSS for dynamic stability enhancement of power system. Journal of Electrical Systems, 13(2):376-386.
[3] Kato Y, Yoda K, Ohtaka T, Iwamoto S [2003] Use of critical clearing time for transient stability preventive control. IFAC Proceedings Volumes, 36(20):1127-1132.
[4] Roberts LGW, Champneys AR, Bell KRW, Di Bernardo M. [2015] Analytical approximations of critical clearing time for parametric analysis of power system transient stability. IEEE Journal on Emerging and Selected Topics in Circuits and Systems, 5(3):465-476.
[5] Vu VTL, Turitsyn K. [2015] Lyapunov functions family approach to transient stability assessment. IEEE Transactions on Power Systems, 31(2):1269-1277.
[6] Hadj Abdallah H, Chtourou M, Guesmi T, Ouali A. [2006] Feedforward neural network-based transient stability analysis of electric power systems. European Transaction on Electrical Power, 16:577–590.
[7] Haidar AMA, Mustafa MW, Ibrahim FAF, Ahmed IA. [2011] Transient stability evaluation of electrical power system using generalized regression neural networks. Applied Soft Computing, 11:3558-3570.
[8] Olulope PK, Folly KA, Chowdhury SP, Chowdhury S. [2011] Prediction of critical clearing time using artificial neural network. IEEE Symposium on Computational Intelligence Applications in Smart Grid (CIASG), Paris-France, 11-15.
[9] Sulistiawati IB, Abdillah M, Soeprijanto A. [2012] Prediction of critical clearing time of Java-Bali 500 KV power system under multiple bus load changes using neural network based transient stability model. International Journal on Electrical Engineering and Informatics, 4(1): 52-66.
[10] Sulistiawati IB, Priyadi A, Qudsi OA, Soeprijanto A, Yorino N. [2016] Critical clearing time prediction within various loads for transient stability assessment by means of the extreme learning machine method. Electrical Power and Energy Systems, 77:345-352.
[11] Yan C, Zhou X. [2019] Online application of solving method for critical clearing time of three-phase short circuit in power system. Power System Technology, 33(17):56-63.
[12] Paul A, Senroy N. [2015] Critical clearing time estimation using synchrophasor data-based equivalent dynamic model, IET Generation. Transmission & Distribution, 9(7):4-30.
[13] Boussahoua B, Boudour M. [2009] Critical clearing time evaluation of power system with UPFC by energetic method. Journal of electrical systems, Special Issue (1), 85-88.
[14] Yorino N, Priyadi A, Kakui H, Takeshita M. [2010] A new method for obtaining critical clearing time for transient stability. IEEE Transactions on Power Systems, 25(3):1620-1626.
[15] Wadduwage DP, Geeganage J, Annakkage UD, Wu CQ. [2013] Investigation of the applicability of Lyapunov exponents for transient stability assessment. 2013 IEEE Electrical Power & Energy Conference, Halifax, Canada.
[16] Dommel HW, Sato N. [1972] Fast transient stability solutions. IEEE Transactions on Power Systems, 91:1643-1650.
[17] McLaren PG, Forsyth P, Perks A, Bishop PR. [2011] New simulation tools for power systems. In: Transmission and Distribution Conference and Exposition IEEE/PES, p. 91-96.
[18] Vu TL, Al Araifi SM, El Moursi MS, Turitsyn K. [2016] Toward simulation-free estimation of critical clearing time. IEEE Transactions on Power Systems, 31(6):4722-4731.
[19] Jafarzadeh S, Genc VMI. [2018] Probabilistic dynamic security assessment of large power systems using machine learning algorithms. Turkish Journal of Electrical Engineering & Computer Sciences, 26:1479-1490.
[20] Zhang Y, Wehenkel L, Rousseaux P, Pavella M. [1997] SIME: A hybrid approach to fast transient stability assessment and contingency selection. Electrical Power and Energy System, 19(9):195-208.
[21] Kundur P, Balu NJ, Lauby MG. [1994] Power system stability and control. McGraw-hill, New York, USA.
[22] Jang JSR. [1993] ANFIS: Adaptive-network-based fuzzy inference system. IEEE Transactions on Systems, Man, and Cybernetics, 23(3):665-685.
[23] Fraile-Ardanuy J, Zufiria PJ. [2007] Design and comparison of adaptive power system stabilizers based on neural fuzzy networks and genetic algorithms. Neurocomputing, 70:2902-2912.
[24] Pai MA. [1989] Energy function analysis for power system stability, Kluwer Academic Publishers, New York,USA.

ARTICLE

SURROUND DIVERGENCE SELF ASSESSED LINEAR REGRESSIVE AND HAMMERSLEY-CLIFFORD DEEP CLASSIFICATION FOR EARLY GLAUCOMA RECOGNITION

Narmatha Venugopal*, Kamarasan Mari

Department of Computer and Information Science, Annamalai University, Tamil Nadu, INDIA

ISSN 0976-3104

ABSTRACT

Glaucoma is an eye disorder that leads to blindness. Most of the research works conducted for early glaucoma detection in the eye fundus images and correspondingly obtain statistical values for early glaucoma detection. However, these statistical based methods rely heavily on optic disc and optic cup ignoring certain fine-tuned (i.e. salient) visual features. In this work, a method called, Self-assessed Linear Regressive segmentation and Hammersley-Clifford Deep Classification (SLR-HCDC)is presented to extract fine-tuned visual features so that glaucoma detection is fastened along with higher rate of sensitivity. First, pre-processing is performed with input retinal fundus images. Second, with pre-processed input retinal images, a Center Surround Divergence Feature extraction model is applied for fine-tuned feature extraction. With the more fine-tuned features extracted, glaucoma detection is said to be fastened. Next, a Self-assessed Linear Regressive segmentation model is applied to the fine-tuned features extracted for performing image segmentation. Here a linear regression is formed between the fine-tuned features to measure self-assessed score for its optic disc segmentation result. Then, the best fit is obtained by applying a self-assessed score with the objective of improving the sensitivity. Finally, Hammersley-Clifford Deep Classification model is applied to the segmented images for early glaucoma detection. Learning of segmented image features are done based on the Gibbs distribution that performs classification between three types of classification at an early stage. To evaluate the performance of the proposed method, three different factors are measured, sensitivity, specificity and accuracy using Digital Retinal Images collected from HRF image database.

KEY WORDS
Glaucoma Detection, Self-assessed, Linear Regressive segmentation, Hammersley-Clifford, Deep Learning

INTRODUCTION

One of the major root causes of blindness all over the world is glaucoma. Glaucoma is an optic neuropathy it correlated with predictable damage to the optic nerve, blindness and patterns of visual impairment which principally includes the loss of retinal ganglion cells (RGCs). The lamina cribrosa is the putative site of retinal ganglion cell axonal injury in glaucoma, where the initial damage appears to be an interruption of normal axoplasmic flow. This is go along with by progressive laminopathy and transsynaptic degeneration. Structural alteration to the RGCs and their axons can be notice clinically as changes in the retinal nerve fiber layer (RNFL) and optic nerve topography can be imaged by computerized devices such as spectral-domain optical coherence tomography (OCT) in the macula, RNFL, optic disc, and lamina, which facilitate diagnosis, monitoring, and treatment. Therefore, there are different types to evolution of computer vision algorithms designed for detecting glaucoma on the basis of the eye fundus images provided as input. But, these algorithms are failed to achieve efficient glaucoma detection in terms of minimum sensitivity and specificity. In order to these existing issues, the proposed Self-assessed Linear Regressive segmentation-based Hammersley-Clifford Deep Classification model is introduced for early glaucoma detection with higher sensitivity and specificity.

A more straightforward and genuine solution for glaucoma detection called, Modified U-Net neural network was presented in [1]. Despite improvement found in segmentation quality, with the optic cup recognition being challenging, the detection of glaucoma was not said to be fastened. Hybrid feature set [2] method provided a novel algorithm for glaucoma detection from digital fundus images. The method included an integration of structural and non-structural features to increase the glaucoma diagnosis accuracy. Though sensitivity and specificity were said to be addressed, early sensitivity with early glaucoma detection was not made.

In [3], glaucoma detection prediction based on statistical analysis was presented. These methods hence provide reliable mechanisms in assisting physicians in disease identification at an early stage. In [4], based on the Regions with Convolutional Neural Network (RCNN), localization and optic disc extraction from a retinal fundus image was made. With the basic consideration of intraocular pressure, a method based on Haralick features [5] were used to differentiate between normal and glaucoma affected retina. Yet another open angle glaucoma was also considered for diagnosis in [6] using a random forest model. In light of the modern achievements of fully convolutional networks (FCNs) tested to biomedical disease diagnosis, the potentiality in the purview of retinal artery-vein was assessed in [7] via deep learning. In [8], with the aid of clinical and technological aid, early glaucoma diagnosis was made using four different artificial intelligence classification methods, namely, multi-layer perceptron, support vector machine, K-nearest neighbor and decision tree. In [9], different Convolutional Neural Networks (CNN) mechanisms were applied to manifest the impact in the implementation of pertinent characteristics like the size of data, use of defined architectures and so on.

A novel deep learning method was introduced in [10] for ophthalmic diagnosing with help of retinal fundus images. However, the improvement of sensitivity and specificity are not sufficient in this method. A weighted path convolution neural network (WP-CNN) was implemented in [11] for diabetic retinopathy (DR)

Received: 9 Mar 2020
Accepted: 21 Apr 2020
Published: 3 May 2020

***Corresponding Author**
Email:
balaji.narmatha8@gmail.com
Tel.: +91-9629832484

IIOAB JOURNAL
ISSN: 0976-3104

identification from eye fundus images. However, the deep learning method does not suitable for large datasets.

Optical coherence tomography evaluation in glaucoma was presented in [12]. Yet another joint method for optic disc and cup segmentation aiding glaucoma detection was presented in [13] using Region-based Convolutional Neural Network (Joint RCNN) towards improving the accuracy of glaucoma detection. Temporally modulated flicker were used in [14] for conducting glaucoma screening test. An automatic diagnosis system based on Pyramid Histogram of Oriented Gradients (PHOG) for glaucoma disease diagnosis was presented in [15]. A review of fundus image classification methods for glaucoma detection was proposed in [16]. However, the cost incurred in disease diagnosis was not concentrated. To address this issue, a cost efficient model based on the revised artificial neural network along with back propagation algorithm was presented in [17]. With higher rate of correlation, disease diagnosis is yet considered to be a tedious process. In [18], a ground truth and evaluation methodology was introduced for automatic detection of diabetic retinopathy.

However, the above mentioned existing methods are having some limitation such as minimum sensitivity, specificity and accuracy during glaucoma detection. Therefore, in this work Self-assessed Linear Regressive segmentation and Hammersley-Clifford Deep Classification (SLR-HCDC) method is designed for early glaucoma detection with higher accuracy.

In this work, instead of directly segmenting the optic disc and optic cup, we propose to extract the fine-tuned features. The extracted fine-tuned features are then segmented for early glaucoma detection based on the feature maps using trustworthiness score. Finally, we propose a Hammersley-Clifford theorem for deep classification using Gibbs distribution with respect to Markov random field for early detection. The main contributions of the proposed SLR-HCDC technique are as follows:

- To improve the specificity rate, Center Surround Divergence Feature extraction algorithm is utilized in the proposed SLR-HCDC technique. A Center Surround Divergence (CSD) operator is used to detect positions that stand out from their surroundings. Feature mapping is based on the center and surround level, statistical evaluation is performed for extracting fine-tuned features from the dataset.

- To increase the sensitivity, the proposed SLR-HCDC technique used the Self-assessed Linear Regressive segmentation model. With help of extracted fine-tuned feature, Self-assessed Linear Regressive image segmentation is performed. Based on the self-assessed trustworthiness score value, best fit is obtained (i.e., sensitivity improved segmented images).

- To enhance the accuracy, the proposed SLR-HCDC technique is introduced. In this technique, Hammersley-Clifford Deep Classification model is used to increase the accuracy of glaucoma disease diagnosis. Based on the Gibbs distribution, the segmented images are identified as normal or glaucoma.

MATERIALS AND METHODS

Self-assessed linear regressive segmentation and hammersley-clifford deep classification

Glaucoma is considered to be one of the most deadly disease whose progression results in permanent blindness. If only detected accurately at an early stage, the progression of glaucoma is said to be stopped. In this work, a Self-assessed Linear Regressive segmentation and Hammersley-Clifford Deep Classification method that enables the physicians in early diagnosis of glaucoma patients with high accuracy and minimum error and complexity is presented. Deep learning classification method is introduced in the proposed technique for accurate disease diagnosis. Deep learning is a category of machine learning algorithms which use deep neural networks to learn different tasks. Machine learning (ML) is a scientific study of algorithms and statistical models that computer systems used to perform a specific task without using explicit instructions, relying on patterns and inference instead. It is seen as a subset of artificial intelligence. [Fig. 1] shows the block diagram of the SLR-HCDC method.

The SLR-HCDC method obtains a raw input retinal fundus image and performs the color conversion. Followed by which Center Surround Divergence Feature extraction model is applied to extract fine-tune features, therefore fastening the glaucoma detection. Next, Self-assessed Linear Regressive segmentation model is applied to the fine-tuned features for obtaining sensitivity improved segmented image with minimum complexity. Finally, deep learning classification using Hammersley-Clifford theorem is performed to predict accurate glaucoma detection. This classification method classifies the images into three types such as glaucoma, non-glaucoma or early detection based on the Gibbs distribution.

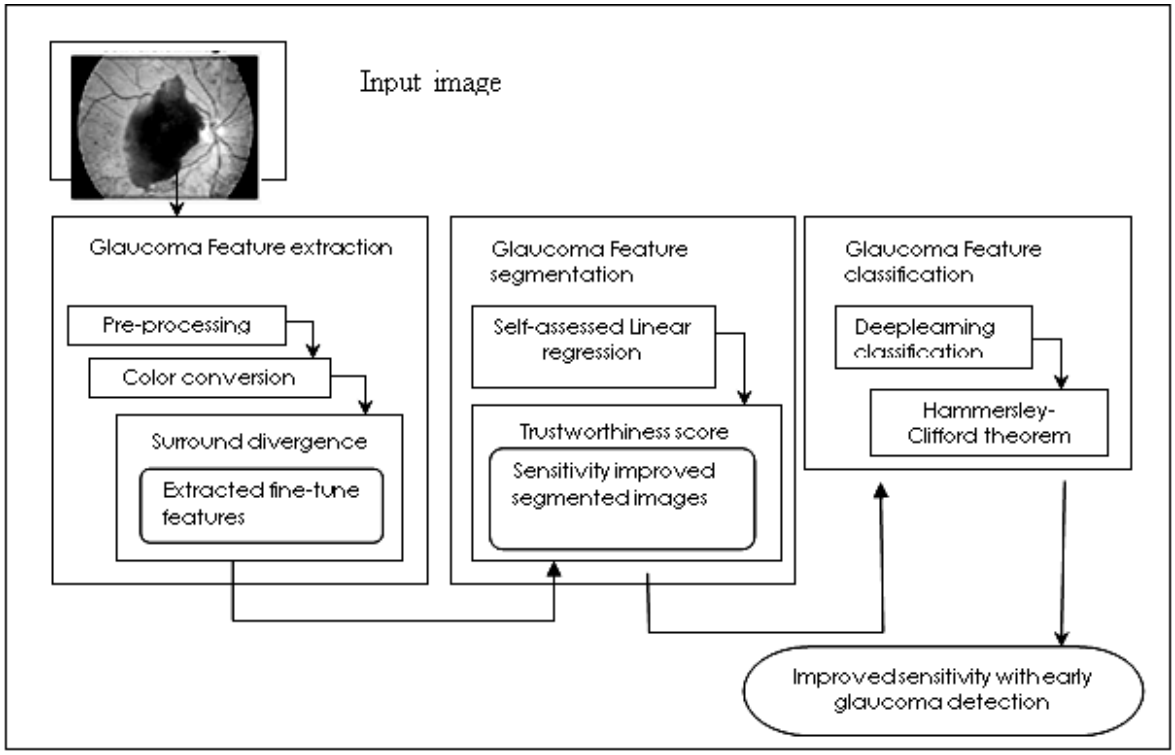

Fig. 1: Block diagram of self-assessed linear regressive segmentation and hammersley-clifford deep classification

Center surround divergence feature extraction model

At first, pre-processing is performed with input retinal fundus images, where color retinal fundus image is converted to corresponding gray image. Next, to the pre-processed retinal fundus image, a Center Surround Divergence Feature extraction model is applied with the objective of extracting fine-tuned features, therefore, fastening the glaucoma being detected.

The input retinal fundus images used for obtaining fine-tuning features were cropped in an automatic manner. To do this pre-processing, the input color retinal fundus image is converted to corresponding gray image. Image pre-processing is done around the optic disc in eye fundus image, it has a clinical reason, that is glaucoma disease affects specifically the optic disc and its surroundings. In this work, to extract fine-tuned features, a Center Surround Divergence (CSD) operator is used to detect positions that stand out from their surroundings.

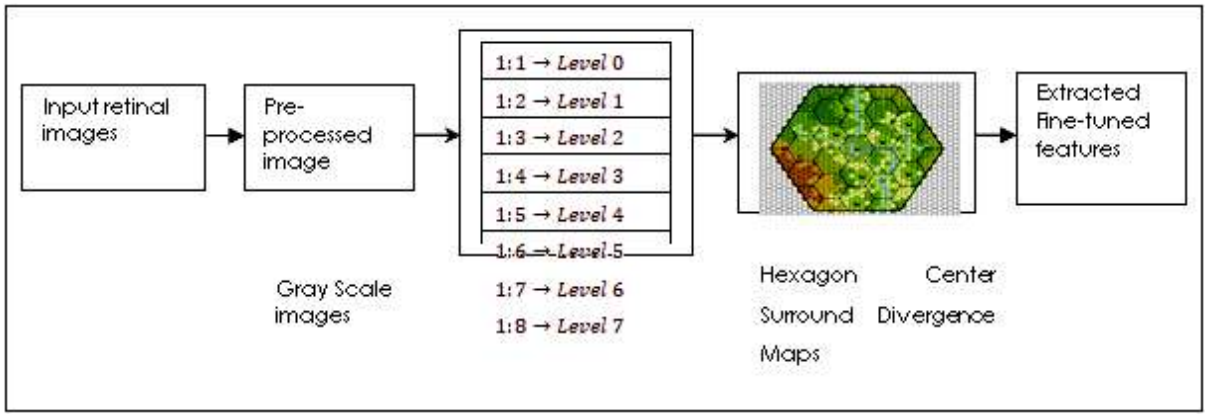

Fig. 2: Center Surround Divergence Feature extraction

The CSD operator is administered as the contrast between finer and coarser scales. [Fig.2] shows the Center Surround Divergence Feature extraction model for extracting fine-tuned features. The Center Surround Divergence Feature extraction involves two steps. The first step involves the intensity identification. The

second step involves the statistical measurement. The pseudo code representation of Center Surround Divergence Feature extraction is given below.

Input: Retinal Fundus Image '$I = I_1, I_2, \ldots, I_n$'
Output: Fine-tuned feature extraction ''
1: **Initialize** finer 'c' and decimated values 'd' 2: **Begin** 3: **For** each Retinal Fundus Image '$I = I_1, I_2, \ldots, I_n$' 4: With finer and decimated values measure tuned level 5: Obtain feature map from surround level to center level 6: Obtain feature map from center level to surround level 7: Identify intensity based on feature maps 8: Measure Center Surround Divergence 9: Obtain statistical values for feature map within super pixel 10: **Return** (fine-tune feature 'FE') 11: **End for** 12: **End**

Algorithm 1: Center Surround Divergence Feature extraction algorithm

Let us assume that the center of the retinal fundus image is a pixel at range 'c ∈{2,3,4}' (i.e. c representing finer level) with 'd ∈{3,4}' (i.e. d representing the decimated value) then surround (i.e. s representing tuned level) being the analogous pixel at scales is mathematically expressed as given below.

$$s=c+d \quad (1)$$

With the above said fine-tuned decimated value, Hexagon maps are empirically obtained at levels

's=(2+3=5,2+4=6,3+3=6,3+4=7,4+3=7,4+4=8)', therefore, 's=2:5,2:6,3:6,3:7,4:7,4:8'. Let us further assume the feature map in center level 'c⟶FM(c)' and feature map in surround level 's⟶FM(s)', then Hexagon Center Interpolation 'HCI' map is mathematically written as given below.

$$HCI(s)\longrightarrow \llbracket FM \rrbracket\_(s\text{-}c)\ [FM(s)] \quad (2)$$
$$HCI(c)\longrightarrow \llbracket FM \rrbracket\_(c\text{-}s)\ [FM(c)] \quad (3)$$
$$HCI(c,s)\longrightarrow [HCI(s)\ \cup HCI(c)] \quad (4)$$

From the above equation (2) and (3), ' 〖FM〗 _(s-c)', represent the feature map from surround level 's', to the center level 'c' and ' 〖FM〗 _(c-s)' represent the feature map from center level 'c' to the surround level 's' respectively. Finally, the intensity 'HCI(c,s)' is identified according to the union of hexagon center interpolation with respect to the surround and center level. The second step involves the identification of feature maps within super pixel. This is performed by applying statistical evaluation. To obtain the statistical evaluation, first, a Center Surround Divergence is measured as given below.

$$CSD\longrightarrow FM(c)\text{-}HCI(s) \quad (5)$$

Followed by the evaluation of center surround divergence factor, the map values are measured from 'r', 'g', 'b', 'h' and 's' and channels to obtain resultant map values as '6*5=30 maps'. Here '6' represents the hexagon and '5' represents the RGB, HS values respectively, with maps represented as 'M_i,i=1,2,...,30'. The 'CSD' features as given above are then measured as the first and second instance of the center (finer) and surround (tune) feature maps within super pixel based on the mean and variance values. They are mathematically evaluated as given below.

$$\mu\_j\ (i)=CSD*\sum\_(p,q \in \llbracket SP \rrbracket\ \_j) \llbracket M\_i\ (p,q) \rrbracket \quad (6)$$
$$\sigma(i)=CSD*\sum\_(p,q \in \llbracket SP \rrbracket\ \_j)[M\_i\ (p,q)-\mu\_j\ (i)]^2 \quad (7)$$

From the above equation (6) and (7), 'μ_j' represents the mean of the feature maps and 'σ' represents the variance of the feature maps within super pixel 'SP' for the corresponding five channels '$RGBHS$'. By this way, the proposed SLR-HCDC technique extracts the fine-tuned features using center surround divergence factor.

Self-assessed linear regressive segmentation model

Next, a Self-assessed Linear Regressive segmentation model is applied to the fine-tuned features extracted. Between the fine-tuned features, a linear regression is formed. With this, self-assessed trustworthiness score is measured for its corresponding optic disc. Finally, the best fit is said to be obtained via a self-assessed score with the objective of improving the sensitivity. Figure 3 shows the Self-assessed Linear Regressive segmentation model.

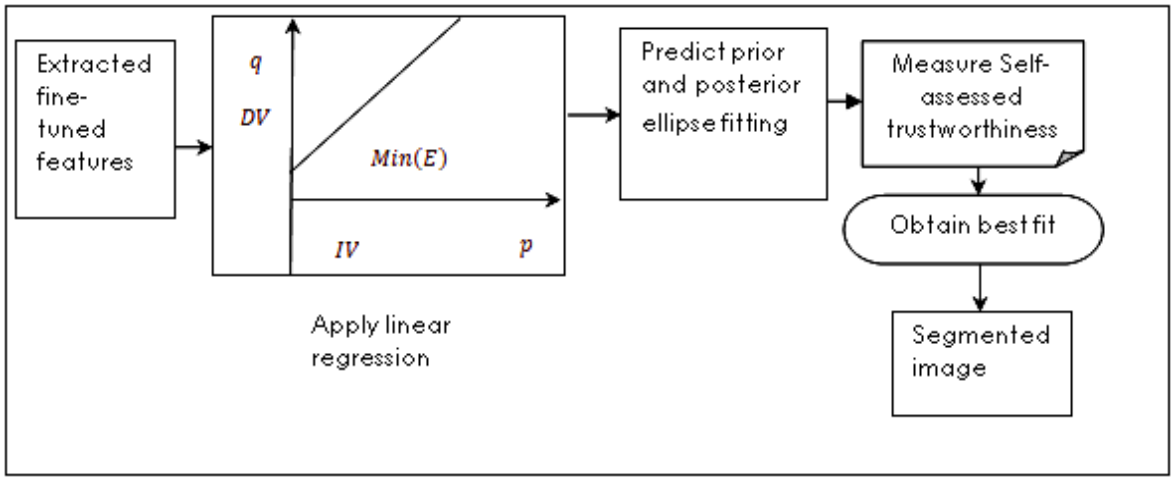

Fig. 3: Self-assessed linear regressive segmentation

As shown in the above figure, fine-tuned features extracted are provided as input. To start with, a linear regression is formed between the fine-tuned features. Here, the x axis or the independent variable 'IV' is represented as 'p' and the y axis or the dependent variable 'DV' is represented as 'q'. As the disc is usually very closer to an ellipse, the resultant boundary acquired prior and posterior ellipse fitting should be nearer if the super pixel based segmentation is nearer to the actual boundary. Otherwise, the result is likely to be less reliable. So first, a linear regressive value is identified to the extracted features so that resultant boundary acquired prior and posterior ellipse fitting are nearer to the actual boundary. Next, self-assessed trustworthiness score is measured with which the best fit obtained is the final segmented image. The algorithm representation of Self-assessed Linear Regressive model is given below.

Input: Fined-tuned Feature Extracted 'FE'
Output: Sensitivity improved segmented image 'SI'
1: Initialize 'b_0', 'b_1' **2: Begin** 3: Predict prior and posterior ellipse fitting nearer to actual boundary 4: Measure the error 5: Measure self-assessed trustworthiness score **6: Return** (Segmented Image 'SI') **7: End**

Algorithm 2: Self-assessed Linear Regressive segmentation

As given in the above Self-assessed Linear Regressive algorithm, the goal is to design a model that can fit nearer to the actual boundary with the given extracted features as input. Using the extracted features, a regression line is obtained that will given minimum error. That is if we give the features extracted as input, our model should predict the prior and posterior ellipse fitting nearer to the actual boundary with minimum error. This is measured as given below.

$$Pred= b\_0+b\_1*FE \quad (8)$$

From the above equation (8), the values 'b_0' and 'b_1' are selected in such a manner that they reduce the error. With the sum of squared error taken as a parameter to measure, then objective is to obtain the prior and posterior ellipse fitting that best reduces the error. This is measured as given below.

$$E= \sum\_(i=1)^n \left[\!\left[(A\_Output- P\_Output)**2\right]\!\right] \quad (9)$$

With the above predicted linear regressive value 'Pred' subject to minimum error 'E', self-assessed score is measured. To obtain the self-assessed trustworthiness score, initially, for each super pixel 'p' in 'P', the nearest feature in 'Q' and their distance is measured as given below.

$$\left[\!\left[Dis\right]\!\right]\_f(p)=INF\{Dis(p,q) \mid q \in Q\} \quad (10)$$

From the above equation (10), 'INF' denotes the infimum and 'Dis(p,q)' representing the distance between the super pixels 'p' and 'q'. Here, infimum refers to the greatest element of the containing set that is smaller than or equal to all elements of the subset. Then, the self-assessment trustworthiness outcome is computed as the ratio of the number of 'p' with ' $\left[\!\left[Dis\right]\!\right]\_f(p)<Th$' to the total number of 'p'. With the assumption that 'Th'

refers to the neuro retinal rim (i.e. the tissue between the border of the cup and the disc), the trustworthiness score is measured as given below.

$$T(p)=Count\{(p|\ 〖Dis〗_f(p)<Th, p\in P)\}/Count(p) \quad (11)$$

Finally, with the above said self-assessed trustworthiness 'T(p)' score, the best fit is obtained for final segmented image. In this manner, segmented retinal image improving the sensitivity is said to be arrived at.

Hammersley-Clifford Deep Classification model

Image classification is the potentiality to distinguish glaucoma, non glaucoma region and early detection by applying feature based image extraction method. Classifiers attain significant results when the principal model applied for separation fits well with the sample distribution of retinal images. In this work, Hammersley-Clifford Deep Classification model is applied to the segmented images for early glaucoma detection. Learning of segmented image features are done based on the Gibbs distribution that performs classification between three types of classification at an early stage such as glaucoma, non glaucoma region and early detection. [Fig.4] shows the schematic diagram of Hammersley-Clifford Deep Classification model. The pseudo code representation of Hammersley-Clifford Deep Classification is given below.

Input: Segmented Images 'SI'
Output: Early glaucoma detection
1: Begin **2:** **For** each Segmented Images 'SI' 3: Measure the weight via Markov random field 4: Measure the step function via Gibbs distribution 5: Postulate Hammersley-Clifford theorem for classification 6: **End for** 7:**End**

Algorithm 3: Hammersley-Clifford Deep Classification

As given in the above classification algorithm, for each segmented images given as input, the objective here remains in early glaucoma detection with minimum errors. A Fully Connected Layer is a layer in which the neurons (i.e. pixels of segmented retinal images) is said to be connected to all the neurons ((i.e. pixels of remaining segmented retinal images) in the preceding layer. This fully connected layer integrates all the features learned by the preceding layers across the image to recognize the larger patterns. The last fully connected layer integrates the feature with the objective of classifying the segmented retinal images into three types.

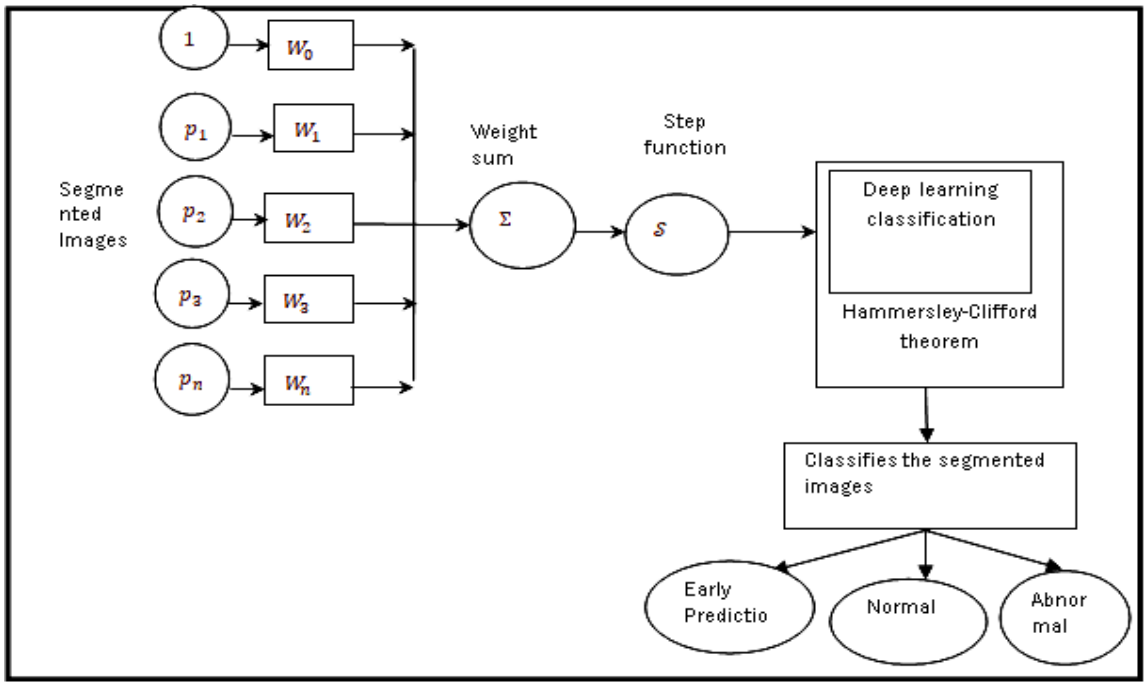

Fig. 4: Deep classification using Hammersley-Clifford theorem

As illustrated in the above [Fig. 4], for each segmented input images, the weights are calculated based on the Markov Random Field. This is mathematically expressed as given below for each center level 'c' and surround level 's'.

$$W(\llbracket SI \rrbracket\_o) = Prob\{P\_s = p\_s \mid P\_c = p\_c, \text{for } s \neq c\} \quad (12)$$

From the above equation (12), the weights 'W' of the corresponding segmented images 'SI' are obtained based on the vector corresponding to center and surround level of each feature maps. The final layer is the classification layer. This classification layer utilizes the Gibbs distribution for each segmented retinal image input to assign the input to one of the mutually exclusive classes.

$$GD = \prod \llbracket V\_SI(p) \rrbracket \quad (13)$$

From the above equation (13), the Gibbs distribution 'GD' refers to a positive function 'V_SI' that depends on 'p' only through the coordinates '{P_s,P_c :s,c∈SI }'. Finally, the classification of three types namely, normal, abnormal or early detection of glaucoma is obtained based on the Hammersley-Clifford theorem. The Hammersley-Clifford Theorem postulates that the process '{P_s,P_c :s,c∈SI }' is a Markov random field if and only if the corresponding 'GD' is a Gibbs distribution. Then, the segmented images are said to be early detection. If the corresponding 'GD' does not forms a Gibbs distribution with respect to Markov random field, then, the segmented images are said to be abnormal. If the corresponding 'GD' is more equivalent with respect to Markov random field, then, the segmented images are said to be normal.

RESULTS

This section of the paper contains comparison between our solution Self-assessed Linear Regressive segmentation and Hammersley-Clifford Deep (SLR-HCDC) and existing methods Modified U-Net neural network [1] and Hybrid feature set [2]. Results are reported for publicly available DIARETDB0 - Standard Diabetic Retinopathy Database [18] obtained from http://www.it.lut.fi/project/imageret/diaretdb0/index.html. The current database comprises of 130 color fundus images, out of which 20 images are found to be normal and 110 images contain certain amount of signs of the diabetic retinopathy. Performances are evaluated for three different parameters, sensitivity, specificity and diagnosis accuracy. The hyper parameter for deep neural network is given as follows,

Table 1: Hyper parameter for deep neural network

Hyper parameter	Value
Learning rate	0.5
Weight	0.44
Hidden layer	5

Clinical tests are said to be evaluated based on the sensitivity and specificity rate. The sensitivity and specificity rate are independent of the population of interest (i.e. samples considered for experimentation) subjected to the test. To conduct the specificity and sensitivity test, both the positive and negative predictive values are useful when considering the value of a test to a clinician. These two rates are dependent on the retinal disease prevalence in the population of interest.

Performance evaluation of sensitivity, specificity and diagnosis accuracy

The sensitivity refers to the ability of the test to correctly identify glaucoma disease. In the example of a medical test used to identify a disease, the sensitivity of the test is the proportion of people who test positive for the disease among those who have the disease. Mathematically, this can be expressed as:

$$Sensitivity = TP/(TP+FN) \quad (14)$$

From the above equation (14), True Positive 'TP' refers to the number images detected as glaucoma, False Negative 'FN' refers to the number of images detected as glaucoma by an expert but detected as normal by the SLR-HCDC method.

Table 2: Tabulation for Sensitivity

Number of images	Sensitivity (%)		
	SLR-HCDC	Modified U-Net neural network	Hybrid feature set
10	0.8	0.7	0.6
20	0.8	0.7	0.6
30	0.8	0.7	0.6
40	0.7	0.6	0.6
50	0.7	0.6	0.6
60	0.7	0.6	0.7
70	0.6	0.6	0.6
80	0.6	0.7	0.6
90	0.7	0.6	0.6
100	0.8	0.7	0.6

As shown in the above [Table.2] representing the sensitivity analysis, experiments are conducted with 100 different retinal fundus images. The reason behind the improvement of sensitivity is due to the application of Center Surround Divergence Feature extraction model. By applying this model, two different functions i.e., center and surround are said to be performed for feature mapping based on the intensity. With this, the sensitivity rate is said to be improved using SLR-HCDC method by 11% compared to [1] and 18% compared to [2].

The specificity refers to the ability of the test to correctly identify the normal retina. Consider the example of a medical test for diagnosing a disease. Specificity of a test is the proportion of healthy patients known not to have the disease, who will test negative for it. Mathematically, this can also be written as,

Specificity= TN/(TN+FP) (15)

From the above equation (15), True Negative 'TN' refers to the number of images detected as normal, False Positive 'FP' refers to the number of images detected as normal by an expert but detected as glaucoma the SLR-HCDC method.

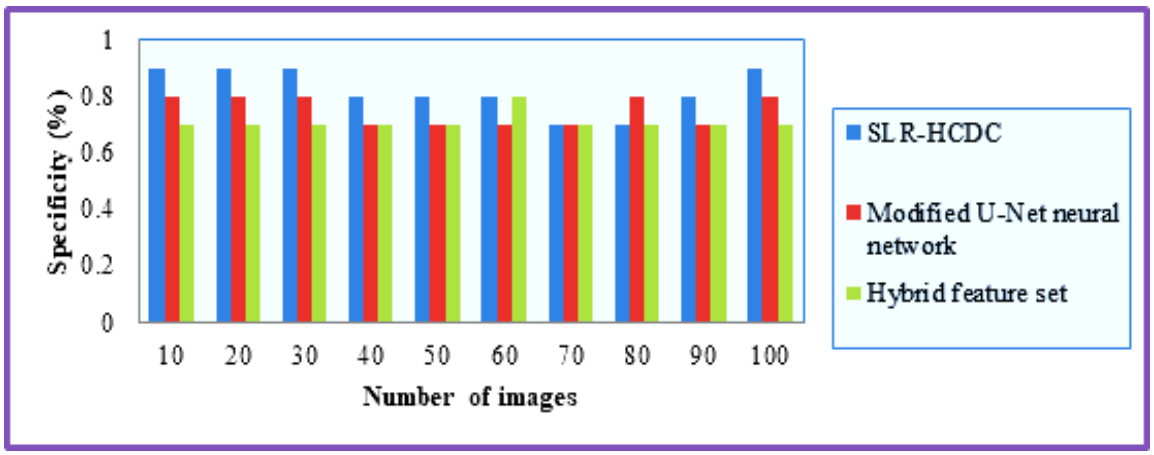

Fig. 5: Performance graph of specificity.

As shown in the above [Fig.5] representing the specificity analysis, experiments are conducted with 100 different retinal fundus images. The specificity rate in the above figure refers to the percentage of patients without having the glaucoma disease correctly identified as not having the condition. The reason behind the improvement of specificity is due to the application of Center Surround Divergence Feature extraction algorithm. By applying this algorithm, feature mapping is performed based on the center and surround level, statistical evaluation is also performed for extracting fine-tuned features. These fine-tuned features are then finally obtained via according to the Center Surround Divergence factor. With this, the specificity rate is said to be improved using SLR-HCDC method by 9% compared to [1] and 16% compared to [2].

The diagnosis accuracy 'A' refers to the percentage ratio of number of retinal images correctly diagnosed as glaucoma images '〖Correct〗_D' to the number of images 'I_i' provided as input for experimentation.

$$A=\sum_{i=1}^{n}[\,〖Correct〗_D/I_i\,]\ 100 \quad (16)$$

Table 3: Tabulation for diagnosis

Number of images	Accuracy (%)		
	SLR-HCDC	Modified U-Net neural network	Hybrid feature set
10	90	80	70
20	90	80	70
30	90	80	70
40	80	70	70
50	80	70	70
60	80	80	70
70	70	70	70
80	70	70	60
90	80	80	70
100	80	70	70

IIOAB JOURNAL
ISSN: 0976-3104

[Table. 3] has given above shows the tabulation of diagnosis accuracy. The comparative analysis shows better diagnosis accuracy using SLR-HCDC method when compared to Modified U-Net neural network [1] and Hybrid feature set [2]. This is because of the application of Hammersley-Clifford Deep Classification. By applying this model, Hammersley-Clifford theorem was applied for Deep Classification that in term uses the Gibbs distribution for each segmented retinal image input to assign the input to one of the mutually exclusive classes. In this way, the diagnosis accuracy using the SLR-HCDC method is found to be better than [1] by 8% and 17% when compared to [2].

DISCUSSION

In this paper, Self-assessed Linear Regressive segmentation and Hammersley-Clifford Deep Classification method introduced for early diagnosis of glaucoma. With pre-processed retinal fundus image, a Center Surround Divergence Feature extraction model is performed in the SLR-HCDC method. Where, the fine-tuned features of pre-processed input image is extracted based on the Hexagon Center Interpolation mapping. Then, the extracted features are applied to the Self-assessed Linear Regressive segmentation model for improving sensitivity of glaucoma detection. In this model, prior and posterior ellipse fitting nearer to the actual boundary is measured for reducing error. Next, with this measured linear regressive value, self-assessed trustworthiness sore value is determined. Based on this score value, extracted features of images are segmented. Finally, Hammersley-Clifford Deep Classification model is used to the segmented images for early glaucoma detection. In this classification model, segmented images are classified into three types such as normal, abnormal and early detection of detection. By this way, the proposed SLR-HCDC method is achieves early glaucoma detection with higher sensitivity and accuracy. In the experimental evaluation, the performance of proposed SLR-HCDC method analyzed with two existing methods namely Modified U-Net neural network [1] and Hybrid feature set [2]. From the experimental analysis, the proposed SLR-HCDC method obtains 72% of sensitivity, 82% of specificity and 81% of accuracy. Similarly, 65% and 61% of sensitivity, 75% and 71% of specificity, 75% and 69% of diagnosis accuracy obtained by existing methods [1] and [2] respectively.

CONCLUSION

In this paper, a Self-assessed Linear Regressive segmentation and Hammersley-Clifford Deep (SLR-HCDC) is presented to detect the glaucoma in retinal fundus images. The proposed method that is based on Deep Classification demonstrated promising performance in diagnosing the glaucoma with considerably higher sensitivity and specificity as compared to existing equivalent methods. The raw images are directly applied to the Center Surround Divergence model to extract fine-tuned features to increase the specificity rate. Fine-tuned features of the glaucoma disease are extracted from center and surround level feature maps. The Self-assessed Linear Regressive used in this study has proved to be an effective strategy for obtaining sensitivity improved segmented image. Finally, by applying Hammersley-Clifford Deep Classification model, higher diagnosis accuracy was said to be achieved. In the experiment the proposed method successfully detected all normal retinal class images correctly and achieved a diagnosis accuracy of 90% Based on the high diagnosis accuracy achieved, the proposed method with a deep classification model can make a relevant improvement to medical science physicians and practitioners by assisting medical image analysis for glaucoma detection. In future, the proposed method is extended for early glaucoma detection with minimum time by using new developed algorithms.

CONFLICT OF INTEREST
There is no conflict of interest.

ACKNOWLEDGEMENTS
The authors are grateful to the authorities of Annamalai University for providing all facilities to carry out this work.

FINANCIAL DISCLOSURE
None.

REFERENCES

[1] Sevastopolsky A. [2017] Optic Disc and Cup Segmentation Methods for Glaucoma Detection with Modification of U-Net Convolutional Neural Network. Pattern Recognition and Image Analysis, 27, 618–662.
[2] Salam AA, Khalil T, Akram MU, Jameel A, Basit I. [2016] Automated detection of glaucoma using structural and non-structural features, Springer Plus, 5(1):1519. doi: 10.1186/s40064-016-3175-4.
[3] Oskarsdottir SE, Heijl A, Bengtsson B. [2019] Predicting undetected glaucoma according to age and IOP: a prediction model developed from a primarily European-derived population. Acta Ophthalmol, 97(4):422-426.
[4] Bajwa MN, Malik MI, Siddiqui SA, et al. [2019] Two-stage framework for optic disc localization and glaucoma classification in retinal fundus images using deep learning, BMC Med Inform Decis Mak, 19, 136
[5] Samanta S, Ahmed SS, Abdel-Megeed MM, Nath SS, et al. [2014] Haralick Features Based Automated Glaucoma Classification Using Back Propagation Neural Network, Proceedings of the 3rd International Conference on Frontiers of Intelligent Computing: Theory and Applications (FICTA) 2014. Advances in Intelligent Systems and Computing, 327.
[6] An G, Omodaka K, Hashimoto K, et al. [2019] Glaucoma Diagnosis with Machine Learning Based on Optical Coherence

Tomography and Color Fundus Images, Journal of Healthcare Engineering, J Healthc Eng, 2019:4061313.
[7] Ruben H, Bart E, Ingeborg S, et al. [2019] Artery–vein segmentation in fundus images using a fully convolutional network, Computerized Medical Imaging and Graphics. Computerized Medical Imaging and Graphics, 76: 101636.
[8] Amine ME, Lazouni MEA, Feroui A, Saïd M. [2019] A new intelligent system for glaucoma disease detection. International Journal of Computer Aided Engineering and Technology 11(4/5):613-632.
[9] Gómez-Valverde JJ, Antón A, Fatti G, et al. [2019] Automatic glaucoma classification using color fundus images based on convolutional neural networks and transfer learning. Biomed Opt Express, 10(2):892-913.
[10] Sengupta S, Singh A, Leopold HA, Gulati T, Lakshminarayanan V. [2019] Ophthalmic Diagnosis Using Deep Learning with Fundus Images - A Critical Review. Artificial Intelligence in Medicine, 102:101758.
[11] Liu YP, Li Z, Xu C, Li J, Liang R. [2019] Referable Diabetic Retinopathy Identification from Eye Fundus Images with Weighted Path for Convolution Neural Network. Artificial Intelligence in Medicine, 99(101694):1-7.
[12] Fortune B. [2019] Optical coherence tomography evaluation of the optic nerve head neuro-retinal rim in glaucoma. Clin Exp Optom,102(3):286-290.
[13] Jiang Y, Duan L, Cheng J, Gu Z, Xia H, Fu H, Li C, Liu J. [2020], JointRCNN: A Region-based Convolutional Neural Network for Optic Disc and Cup Segmentation. IEEE Trans Biomed Eng, 67(2):335-343.
[14] Fidalgo BR, Jindal A, Tyler CW, et al. [2018] Development and validation of a new glaucoma screening test using temporally modulated flicker. Ophthalmic Physiol Opt, 38(6):617-628.
[15] Gour N, Khanna P. [2019] Automated Glaucoma Detection using GIST and Pyramid Histogram of Oriented Gradients (PHOG) descriptors. Pattern Recognition Letters, 10.1016/j.patrec.2019.04.004
[16] Saba T, Bokhari STF, Sharif M, et al. [2018] Fundus image classification methods for the detection of glaucoma: A review. Microsc Res Tech, 81(10):1105-1121.
[17] Pavithra G, Manjunath TC, Lamani D. [2019] Detection of Primary Glaucoma Using ANN with the Help of Back Propagation Algo in Bio-medical Image Processing, doi:10.1007/978-3-030-28364-3_5.
[18] Kalesnykiene V, Kamarainen JK, Lensu L, et al. [2006] DIARETDB0: Evaluation Database and Methodology for Diabetic Retinopathy Algorithms, Technical report. Technical report, Lappeenranta University of Technology, Finland, 2006. 6.

IIOAB JOURNAL

ARTICLE

PHARMACOLOGICAL REGULATION OF THE DETOXICATION FUNCTION OF POULTRY LIVER IN MYCOTOXICOSIS

Eugeny P. Dolgov*, Elena V. Kuzminova, Marina P. Semenenko, Denis V. Osepchuk, Ksenia A. Semenenko, Andrey A. Abramov

Department of Pharmacology, Federal State Budgetary Scientific Institution, Krasnodar Scientific Center for Animal Husbandry and Veterinary Medicine, Pervomayskaya St., Znamensky, Krasnodar, 350055, RUSSIA

ISSN 0976-3104

ABSTRACT

The article presents the results of studying the effectiveness of pharmacocorrection of combined poultry mycotoxicosis with polysaccharide and phospholipid substances. In an experimental simulation of mycotoxicosis, quails were fed with feed contaminated with aflatoxin B1 in concentration of 0.019 mg/kg of feed and T-2 toxin in concentration of 0.095 mg/kg of feed for a month. For pharmacocorrection of toxicosis, a complex consisting of beet pulp and rapeseed lecithin in 4:1 ratio was used. Poultry of the first experimental group daily got an antitoxic complex at a dose of 2.5 grams per head. The second group received only toxic feed without treatment; the third group got the main diet. The results of the experiment showed that in the group with the use of the antitoxic complex in poultry, an increase in body weight was noted, whereas in the group without treatment on the background of the development of mycotoxicosis negative dynamics of body weight was recorded with a difference of 18.5%. In the group without treatment on 16th, 21st, and 28th days of the experiment 19% of quail deaths were recorded, while the use of the antitoxic complex ensured 100% safety of the poultry. Laboratory studies have shown an increase in the activity of aminotransferases, indicating damage of the membranes of hepatocytes leading to the release of intracellular substances into the bloodstream during intoxication. This process was accompanied by activation of lipid peroxidation with a dominant increase in malondialdehyde (MDA) in poultry blood serum. The use of the complex of polysaccharide and phospholipid substances in experimental mycotoxicosis has the hepatoprotective effect and improves the lipoperoxidation processes in poultry.

KEY WORDS
liver, detoxification, quails, mycotoxicosis, plant fiber, phospholipids

INTRODUCTION

Liver functions in the organism are very diverse, since liver is the central organ of chemical homeostasis, where a single energy pool for the metabolism of carbohydrates, proteins, fats, vitamins, microelements and other substances is created. The barrier function of liver is of a great importance, because many toxic substances of endogenous and exogenous origin are delayed or changed and excreted. The most dangerous of the natural toxicants – pollutants of agricultural raw materials and food products – are microscopic fungi and their toxins – mycotoxins. The most common mycotoxins found in feed are produced by three genera of fungi – *Aspergillus, Penicillium and Fusarium*, and often their content in the feed does not exceed the maximum permissible level. Moreover, numerous studies have proved that many of them even in low concentrations have mutagenic, teratogenic, carcinogenic and immunosuppressive properties, and are also able to reduce the body's resistance to infectious and invasive diseases [1-3].

Mycotoxins contaminate food and feed at all stages of their production, transportation, storage, processing and implementation. In this regard, along with the measures aimed at preventing the entry of mycotoxins into the body, finding ways to reduce the toxicity of xenobiotics already in the gastrointestinal tract is important [4, 5].

Received: 11 Feb 2020
Accepted: 7Apr 2020
Published: 5 June 2020

Among the most promising ways in this area is the use of dietary fiber from recycled plant materials, reinforced with components with hepatoprotective, detoxification and anti-inflammatory activity [6].

For the purpose of primary sorption of toxicants in the gastrointestinal tract, the use of beet pulp, which contains a complex of soluble and insoluble dietary fiber, is proposed. The first include polysaccharides – pectins with the high absorption capacity against heavy metals, mycotoxins and other xenobiotics. The second fraction is represented by insoluble "rough" dietary fiber, which, passing through the gastrointestinal tract, affects intestinal motility and helps to mechanically remove toxic substances from the body [7, 8].

Essential phospholipids are included in compounds obtained from plant resources and possessing high biological activity, including hepatoprotective activity, which led to the inclusion of phospholipid component in the form of rapeseed lecithin in the antitoxic complex [9].

The purpose of the research was to study the pharmacological correction efficiency of combined poultry mycotoxicosis with a complex of polysaccharide and phospholipid substances.

MATERIALS AND METHODS

Studies were carried out on quails of Texas Pharaoh breed with the body weight of 315.7 ± 1.18 g, divided into three groups (two experimental groups and control group) of 16 quails each. In the experiments, quails

***Corresponding Author**
Email:
e.p.dolgov@mail.ru

IIOAB JOURNAL
ISSN: 0976-3104

that passed the quarantine regime and did not have external signs of disease were used. To obtain statistically reliable results, groups were formed according to the principle of paired analogues.

The essence of the method of reproducing combined mycotoxicosis: for 30 days the quails of the experimental groups were fed with the feed naturally contaminated with mycotoxins. The concentration of aflatoxin B1 in samples was 0.019 mg/kg, and concentration of T-2 toxin was 0.095 mg/kg. It should be noted that both toxins separately did not exceed the maximum permissible level, but their combined effect on the body for a long time causes the development of toxicosis. The third group served as an intact control.

Pharmacological correction

For pharmacocorrection of mycotoxicosis a complex of polysaccharide (beet pulp) and phospholipid substances (rapeseed lecithin) was used in 4:1 ratio. The presence of the first component – vegetable fibers from the sugar beet, including pectin and cellulose, determines the ability of the preparation to form complexes with xenobiotics and remove them from the body, as well as to improve the functional state of the gastrointestinal tract due to prebiotic properties. The second component of the preparation, represented by rapeseed lecithin, allows restoring the phospholipid skeleton of the hepatocyte membrane, reducing the intensity of lipid peroxidation processes, the generation of active oxygen metabolites, and eliminating the disturbance of cell energy supply.

The poultry of the first experimental group daily got an antitoxic complex *per os* at a dose of 2.5 grams per head. The second group received only toxic feed without treatment, the third group was kept on the main diet, receiving benign compound feed. All quails could freely take water from automatic drinkers.

Clinical observation

All quails were monitored, weighing was carried out on 15th and 30th days of the experiment. In order to study the effect of the antitoxic complex on the detoxification function of poultry liver, blood was taken from 5 quails from each group for biochemical studies (15 days from the beginning of the experiment and one day after the last use of the complex). Laboratory studies were carried out on a Vitalab Flexor automatic biochemical analyzer using aspartate aminotransferase (AST) and alanine aminotransferase (ALT). The intensity of lipid peroxidation (LPO) was evaluated spectrophotometrically by the level of diene conjugates (DC), ketodienes (KD) and malondialdehyde (MDA).

Statistical processing

Statistical processing of the results was carried out using special software packages. The study of quantitative traits was carried out by comparing the average values of two sample sets with the determination of Student's criterion and significance level (p).

RESULTS

As the result of the studies, it was found out that in the group using the antitoxic complex in poultry an increase in the body weight was noted, while in the group without treatment on the background of the development of mycotoxicosis, negative dynamics of body weight was recorded [Table 1].

Table 1: Influence of the antitoxic complex on quail body weight at mycotoxicosis (M±m; n=16)

Groups	Body weight, g		
	Background	On the 15th day of experiment	On the 30th day of experiment
1 experimental	315.2±1.26	323.8±1.09	334.1±0.86*
2experimental	315.1±1.18	298.7±1.76	282.0±0.93
3 control	317.1±0.87	336.3±1.48	358.0±0.97

Note: * p≤0.05 – the differences are significant in relation to the group without treatment

On the 15th day of research, in the 1st group the body weight of quails increased by 2.7%, while in the 2nd group there was a decrease in weight by 5.2%. On the 30th day of the experiment, the body weight of quails of the 1st group increased by 5.9% in relation to the initial data, with a dynamic decrease in body weight of poultry of the 2nd group by 10.8%. The significant difference between the group using the antitoxic complex and the group without treatment was 18.5%. At the same time, an intact poultry had a dynamic increase in body weight, which was 6.1% by the middle of the experiment and 12.9% at the end of the experiment.

Clinical studies determined that the first symptoms of intoxication in quails of the 2nd group (without treatment) were observed already on the 8th day of the experiment (severe inhibition, decreased egg laying,

narrowing of the palpebral fissure, excretion of serous outflows from the nose and eyes, moderate decrease in appetite).

By the 15th day of the experiment, poultry in this group showed a significant decrease in appetite, increased thirst, watery consistency of greenish droppings, with an admixture of blood, lack of egg laying, as well as egg molding was observed in some quails, and the shell of eggs was soft, deformed and green.

In the group without treatment, on the 16th, 21st and 28th days of the experiment the death of three quails was recorded (18.8% of the total amount). In the group with the use of the antitoxic complex, the safety of quails during the period of the experiment was 100%, and the clinical signs of intoxication (dullness of feathers, decrease in egg laying and weight gain) began to appear only in the middle of the experiment. Moreover, by the end of the experiment, the use of the complex contributed to a significant improvement in the state of the poultry, since there were practically no external signs of intoxication.

Results of biochemical studies

A biochemical blood test found out that with the development of mycotoxicosis, a significant change in the activity of enzymes-markers of the liver condition occurred [Table 2].

In the 2nd group (without treatment), by the middle of the experiment an increase in AST activity by 18.5% was revealed relative to the intact poultry, and at the end of the experiment, the differences between the groups were 28.1%. ALT activity increased more significantly – on the 15th day it increased in 1.7 times and on the 30th day it increased in 1.6 times compared with the indicators obtained in the control group.

Table 2: Influence of the antitoxic complex on the biochemical parameters of quails at mycotoxicosis (M±m; n=5)

Indicators	Groups		
	1 experimental	2 experimental	3 control
	15thday of the experiment		
AST, U/l	319.6±5.43*	365.2±5.19	308.2±2.16
ALT, U/l	22.8±0.85**	27.9±0.74	16.2±0.92
$DC_{(232)}$, AU	0.587±0.03*	0.721±0.06	0.392±0.05
$KD_{(273)}$, AU	0.481±0.05	0.575±0.02	0.417±0.01
$MDA_{(537)}$, μM /l	2.08±0.14*	2.55±0.11	1.34±0.09
30thday of the experiment			
AST, U/l	310.5±5.66*	393.3±4.45	307.1±2.46
ALT, U/l	19.6±0.77**	28.6±1.30	17.5±1.13
$DC_{(232)}$, AU	0.528±0.04***	0.794±0.09	0.383±0.07
$KD_{(273)}$, AU	0.473±0.01**	0.627±0.05	0.403±0.04
$MDA_{(537)}$, μM /l	1.82±0.09***	3.63±0.17	1.29±0.11

Note: (*p≤0.05; ** p≥0.01; ** p≥0.001) the differences are significant in relation to the group without treatment

In quails of the 1st group receiving the antitoxic complex, the activity of AST by the middle of the experiment was lower by 14.3% than the values of the same indicator in the 2nd group, and by the end of the experiment it was lower by 26.6%, but at the same time it exceeded the values obtained from the control group of poultry. A similar dynamics was observed in the ALT concentration, since the significant difference on the 15th day of observation was 22.4% and on the 30th day of the study it was 45.9%, relative to the quail of the 2nd group, but remained higher than the corresponding indicator of the intact quails.

Quail intoxication was accompanied by an increase in LPO processes, which was confirmed by an increase in all lipoperoxidation products. The differences between the intact poultry of the 3rd group and the quails of the 2nd experimental group (without treatment) in the middle of the experiment amounted in the following values: DC – 83.9%, KD – 37.9% and MDA – 1.9 times, and by the end of the experiment DC – 2.1 times , KD – 55.6%, and MDA – 2.8 times, respectively.

The pharmacological effectiveness of the antitoxic complex was manifested in the preventive effect on the development of pathological LPO generation under the influence of mycotoxins. The difference between the quails of the 1st and 2nd groups in the middle of the experiment was: by DC – 22.8%, by KD – 19.6%, and by MDA – 22.6%; by the end of the experiment the difference was: by DC – 50.4%, by KD – 32.6% and by MDA – 2 times.

DISCUSSION

The results of our studies confirm the data that the combined effect of mycotoxins in doses below the maximum permissible level leads to the development of clinical mycotoxicosis in poultry [10, 11]. Aflatoxin and T-2 toxin, when interacting, exhibit synergistic toxicity, causing mortality and decrease in weight gain of quails. These effects were demonstrated in a number of studies on broiler chickens regarding ochratoxin A, aflatoxin and T-2 toxin, which indicated that in most cases, a significant decrease in body weight in poultry

IIOAB JOURNAL
ISSN: 0976-3104

from the second week of the experiment was observed [12-14]. Our results are partially consistent with these data, since in the group without the antitoxic treatment, on the background of prolonged intake of mycotoxins, a constant decrease in body weight of quails was recorded without a dominant manifestation over the periods.

Mycotoxins can induce oxidative stress. In experimental mycotoxicosis in poultry, an increase in the products of lipid peroxidation in the body was revealed starting from the 7th day of the experiment, as well as during the final sampling, by 21st day [15, 16]. Received data indicate that at intoxication of quails with aflatoxin and T-2 toxin the maximum accumulation of lipid peroxidation products occurred at the end of the experiment – on the 30th day with a dominant increase in MDA in poultry blood serum.

Given the diversity of mycotoxin structures, it is necessary to combine different strategies for the treatment and prevention of mycotoxicosis. The most famous method of decontamination of mycotoxins is the use of adsorbents or enterosorbents, which can have organic or inorganic (mainly clay minerals) nature. Numerous studies in animals have reported that aluminosilicates are effective as adsorbents for mycotoxins [17, 18].

We used a new way in the fight against mycotoxicosis in the treatment of diverse substances obtained from natural resources. The studies proved the effectiveness of the complex of substances of polysaccharide and phospholipid nature at combined poultry mycotoxicosis. This effect is confirmed by the previously determined pharmacological properties of lecithin and plant fibers during intoxication, manifested by their ability to regulate the toxicokinetics of heterogenous compounds, including the stages of absorption, hepatic-intestinal recirculation, biotransformation and detoxification [19-23].

CONCLUSION

Thus, the results of the experiment allow us to conclude that during mycotoxin intoxication in quails, the activity of aminotransferases increases, indicating damage of the membranes of hepatocytes leading to the release of intracellular substances into blood. This process is accompanied by the activation of lipid peroxidation. The use of the complex of substances of the polysaccharide and phospholipid nature improves lipoperoxidation and the state of liver of poultry contaminated with mycotoxins, which is manifested by an increase in the safety and weight gain of quails, as well as by a decrease in the clinical manifestations of intoxication.

CONFLICT OF INTEREST

The authors declare no competing interests in relation to the work.

ACKNOWLEDGEMENTS

The study was funded by the Russian Foundation for Basic Research according to the research project No. 19-316-90029.

FINANCIAL DISCLOSURE

None.

REFERENCES

[1] Ivanov AV, Fisinin VI, Tremasov MYa, Papunidi KKh. [2010] Mycotoxicosis (biological and veterinary aspects). Kolos, Moscow. 392 p.
[2] Fisinin VI, Suray PF. [2012] Mycotoxins and antioxidants: an irreconcilable fight. Ochratoxin A. Compound feed, 3: 55-60.
[3] Streit E, Naehrer K, Rodrigues I, Schatzmayr G. [2013] Mycotoxin occurrence in feed and feed raw materials worldwide: long-term analysis with special focus on Europe and Asia. Journal of the Science of Food and Agriculture, 93 (12): 2892-2899.
[4] Tyapkina EV, Khakhov LA, Semenenko MP, Kuzminova E.V. et al. [2014] The basic principles of animal therapy at poisoning. Krasnodar Scientific Center for Animal Husbandry and Veterinary Medicine, Krasnodar. p29.
[5] Grizzle JM, Kersten DB, McCracken MD, Houston AE, Saxton AM. [2004] Determination of the acute 50% lethal dose T-2 toxin in adult bobwhite quail: additional studies on the effect of T-2 mycotoxin on blood chemistry and the morphology of internal organs. Avian Dis., 48: 392-399.
[6] Kornen NN, Viktorova EP, Evdokimova OV. [2015] Methodological approaches to creating healthy nutrition. Nutrition issues, 84(1): 95-99.
[7] Voskoboinikov VA, Tipiseva IA. [2004] About the classification of dietary fiber. Food ingredients. Raw materials and additives, 1: 18-20.
[8] Ipatova LG, Kochetkova AA, Nechaev AP. et al. [2007] Dietary fiber in food products. Food industry, 5: 8-10.
[9] Ushkalova EA. [2003] The place of essential phospholipids in modern medicine. Farmateka, 10(73): 10-15.
[10] Oliveira HF, Souto CN, Martins PC, Di Castro IC, Mascarenhas AG. [2018] Mycotoxins in broiler production. Revista de Ciências Agroveterinárias, 17(2): 292-299.
[11] Di Gregorio MC, de Neeff DV, Jager AV, Corassin CH, de Pinho Carão ÁC, de Albuquerque R, de Azevedo AC, Oliveira CAF. [2014] Mineral adsorbents for prevention of mycotoxins in animal feeds. Toxin Reviews, 33(3): 125-135.
[12] Indresh HC, Umakantha B. [2013] Effect of a combination of ochratoxin and T-2 toxin on productivity, biochemical and immune status of commercial broilers. Veterinary World, 6 (11): 945-949.
[13] Kipper M. et al. [2020] Assessing the implications of mycotoxins on productive efficiency of broilers and growing pigs. Sci. agric., 77 (3): 1-8.
[14] Farooqui MY, et al. [2019] Aluminosilicates and yeast-based mycotoxin binders: Their ameliorated effects on growth, immunity and serum chemistry in broilers fed aflatoxin and ochratoxin. S. Afr. j. anim. sci., 49 (4):619-627.
[15] Yang L, Yu Z, Hou J, Deng Y, Zhou Z, Zhao Z, Cui J. [2016] Toxicity and oxidative stress induced by T-2 toxin and HT-2 toxin in broilers and broiler hepatocytes. Food Chem. Toxicol., 87: 128-137.

[16] Bócsai A, Ancsin ZS, Fernye CS, Zándoki E, Szabó-Fodor J, Erdélyi M, Mézes M, Balogh K. [2015] Dose-dependent short-term effects of T-2 toxin exposure on lipid peroxidation and antioxidant parameters of laying hens. Eur Poult Sci., 79:115.
[17] Grenier B, Oswald I. [2011] Mycotoxin co-contamination of food and feed: meta-analysis of publications describing toxicological interactions. World Mycotoxin Journal, 4(3): 285-313.
[18] Murugesan GR, Ledoux DR, Naehrer K, et al. [2015] Prevalence and effects of mycotoxins on poultry health and performance, and recent development in mycotoxin counteracting strategies. Poult Sci., 94(6): 1298-1315.
[19] Poznyakovsky VM, Chugunova OV, Tamova MYu. [2017] Food ingredients and dietary supplements. Moscow: INFRA-M.143 p.
[20] Ivashev MN et al. [2013] Biological activity of compounds from plant sources. Basic research, 10 (7): 1482–1484.
[21] Greig FH, Kennedy S, Spickett CM. [2012] Physiological effects of oxidized phospholipids and their cellular signaling mechanisms in inflammation. Free Radical Biology and Medicine, 52(2): 266-280.
[22] Frühwirth GO, Loidl A, Hermetter A. [2007] Oxidized phospholipids: from molecular properties to disease. Biochimica et Biophysica Acta (BBA) – Molecular Basis of Disease, 1772(7): 718-736.
[23] Vance, JE, Tasseva G. [2013] Formation and function of phosphatidylserine and phosphatidylethanolamine in mammalian cells. Biochim. Biophys. Acta., 1831: 543-554.